Vol. 2 June, 1957 No. 2

MINERALOGICAL JOURNAL

CONTENTS

Synthesis, Crystal Lattices and Some Electrical Properties of Indium Tellurides and Selenides ..... S. Sugaike... 63

The Interpretation of X-Ray Powder Diffraction Patterns of the Szaibelyite-Sussexite Series ..... Y. Takéuchi... 78

The Absolute Structure of Ullmanite, NiSbS..... Y. Takéuchi... 90

Nacrite-bearing Kaolin Clay from the Kasuga Mine, Kagoshima Prefecture, Japan..... M. Tokunaga ...103

On Probable Eliptic Vibration of Light in Heikolite..... ..... T. Shoda...114

Short Communications

Natural Occurrences of Zeunerite.....K. Henmi...134

Abstract of the Kobutsugaku Zasshi, Journal of the Mineralogical Society of Japan, Vol. 3, No. 2 139

The Mineralogical Society of Japan

Department of Geology and Mineralogy, Faculty of Science, Hokkaido University, Sapporo, Japan

MINERALOGICAL JOURNAL

published by

The Mineralogical Society of Japan

EDITORIAL BOARD

Zyunpei HARADA, *Hokkaido University;* Teiichi ITO, *University of Tokyo;* (Chief) Nobuo KATAYAMA, *University of Tokyo;* Keiichi OMORI, *Tohoku University;* Ryôiti KIRIYAMA, *University of Osaka;* Seitaro TSUBOI, *University of Tokyo;* Takeo WATANABE, *University of Tokyo;* Toyofumi YOSHIMURA, *Kyushu University.*

Instructions to Contributors

Manuscripts of articles should be submitted to the executive editor, Nobuo Katayama, at the College of General Education, University of Tokyo, Komaba, Meguro-ku, Tokyo. The manuscript should be type-written with double space lines, and not exceed 20 sheets of normal type-writing paper. References of literature should be in accordance with the forms used in the pages of this journal.

Plates and figures should be capable of reduction to not more than 10 by 15 centimetres. Line drawings should be in black India ink on white drawing board, tracing paper, or coordinate paper printed in blue. Photographs should be positive glossy prints.

Two referees chosen by the Editorial Board read the manuscript of article submitted before it is accepted for publication.

Thirty reprints without cover will be furnished to the author free of cost and without previous notice from him. Additional reprints will be furnished at cost when ordered.

The price of the journal to subscribers in Japan is 250 yen for a single copy (including postage), and to subscribers in other countries $ 1.00 (including postage) for a single copy, or $ 5.00 (including postage) per volume of 6 numbers.

Printed in Japan

MINERALOGICAL JOURNAL, VOL. 2, No. 2, pp. 63-77, JUNE, 1957

SYNTHESIS, CRYSTAL LATTICES AND SOME ELECTRICAL PROPERTIES OF INDIUM TELLURIDES AND SELENIDES

SUEZO SUGAIKE

Matsuda Research Laboratory,
Tokyo Shibaura Electric Company

ABSTRACT

The crystals of indium tellurides and selenides, InTe, In_2Te_3, $InTe_3$, InSe and In_2Se_3, have been synthesized by the double-furnace technique and their crystal lattices have been characterized by X-ray single crystal examinations.

From the results of their electrical conductivity measurements it has been found that all of them are semiconductors, In_2Te_3 and InSe being poorly conductive with some ionic character, InTe, $InTe_3$ and In_2Se_3 having rather higher conductivities of order of $1 \sim 1 \times 10^2$ $(\Omega\ \mathrm{cm})^{-1}$ at room temperature, and that In_2Se_3 shows a peculiar phase transition at 200°C.. The lattice symmetries of these compounds have been compared with those of other III b metal chalcogenides.

Introduction

The chalcogenides of the III b metals in the periodic table have first been studied by W. Klemm and H.U. von Vogel[8] in 1934. Although the majority of the compounds have been investigated crystallographically by H. Hahn[2)~5)] and by S. Schubert[16], the data on $InTe_3$ and InSe are missing yet.

From the crystal-chemical view-point it will be interesting to see the similarity as well as difference of the properties of In_2Se_3 and In_2Te_3. The electronegativity differences Δx of indium decrease gradually from 1.2 against sulphur, to 1.1 against selenium and 0.8 against tellurium. These small values of Δx suggest, according to Pauling's theory[14], their indium compounds to be valence crystals or semiconductors, with the smallness of Δx indicating the maximum amount (to the extent of 20%) of ionic character of the bonds.

In order to see the bonding character of these compounds, in ad-

dition to the X-ray single crystal examinations, their electrical conductivities were measured as usual using single crystals.

Synthesis

There are two methods for preparation of indium selenides and tellurides: In the "wet" method, InSe, for example, is obtained by applying hydrogen selenide (H_2Se) on molten indium metal, and in the "dry" method, on the other hand, the same compound is prepared by direct fusion of the stoichiometric mixture of the component substances corresponding to the chemical formula. We have adopted the latter method because of its ease of obtaining larger single crystals. The double-furnace technique have been applied after W.D. Lawson[10].

As the starting materials, we used indium metal from New Metal Co. in England guaranteed 99.99% purity, and tellurium and selenium metals spectroscopically examined in our laboratory.

The transparent fused quartz crucible (ca. 1 cm. in diameter), the stoichiometric mixture of two components within, was evacuated and then sealed off by oxy-hydrogen flame. Since it was inevitable that small amounts of selenium or tellurium were sublimated from the mixture and condensed immediately above the sealed point, a slight amount of tellurium or selenium in excess to the calculated amount was usually added. Moreover, as the vapour pressure of molten liquid of selenide was so high at the maximum heating temperature that the crucible of 1.0mm. wall thickness was often damaged, accordingly a double quartz crucible was used. The procedures otherwise were identical with those used in the preparation of In_2Te_3 crystals previously reported[7].

In preparing $InTe_3$ crystals, as they were not homogeneous phase but peritectic when the melt of the stoichiometric mixture was slowly cooled in the ordinary experimental conditions, tellurium was added in excess to the stoichiometric proportion so that the $InTe_3$ crystals were primarily crystallized out from the melt leaving the

residue richer in tellurium. This procedure yielded the aggregate for the most part of coarse $InTe_3$ crystals.

Electrical measurements of the prepared crystals

Determination of electrical conductivity was made using a D.C. potentiometer. Current was passed through the specimens (ca. 10× 3×1 mm. in most compounds) from gold electrodes plated on them through the process of evaporation. The conductivity was determined by measuring the voltage between a pair of platinum probes fixed by compression near both ends of each specimen, and the temperature was measured with a platinum-platinum 13% rhodium or a cupper-constantan thermocouple. All the measurements in high temperature were carried out in an atmosphere of nitrogen gas or *in vacuo* to reduce to minimum the irreversible effects caused by the oxidation of specimens.

Usually the electrical properties of a semiconductor are affected to a considerable extent by crystal imperfections caused, for instance, by impurities, however slight they may be. But the research program here reported was mainly limited to inquiring the "intrinsic" properties of compound that is assumed to be semiconductive and those possibly arising from the peculiar crystal structure. Therefore, the values of the energy gap, which should correspond to the breadth of the forbidden band between the empty and the filled valence band, have been estimated from the temperature dependence of the electrical conductivities, applying the following relation:

$$\sigma=\sigma_0 \exp(-\Delta E/2kT)$$

where σ is the specific electrical conductivity at the absolute temperature $T°$, k the Boltzmann's constant, and ΔE the activation energy of charge carriers in the intrinsic electric conduction state or the energy gap.

Further, in order to confirm an abrupt conductivity change in In_2Se_3 found by the conductivity measurement, the temperature dependence of thermoelectric motive forces were measured by means

of an experimental procedure after H.K. Henisch and M. Francois[6], the temperature difference across the specimen being maintained within 5~8°C..

Researches on individual products

I. *Indium tellurides.* There are four known indium tellurides[17]: In_2Te, InTe, In_2Te_3 and $InTe_3$, of which In_2Te being a peritectic compound, was not studied here.

(1) **InTe.** K. Schubert, E. Dorre and M. Kluge[16] have synthesized this telluride by the dry method in vacuum and determined its crystal structure to be of the TlSe type with $a_0=8.42_0\pm0.005$, $c_0=7.12_5\pm0.005$kX., and $c_0/a_0=0.84_5\pm0.005$. We have taken X-ray photographs of the crystals synthesized by us and confirmed their results.

InTe crystal has splendent lustre and cleaves rather perfectly after {110} making, when cleaved, a prism elongated parallel to the c axis. Colour and streak are lead-grey.

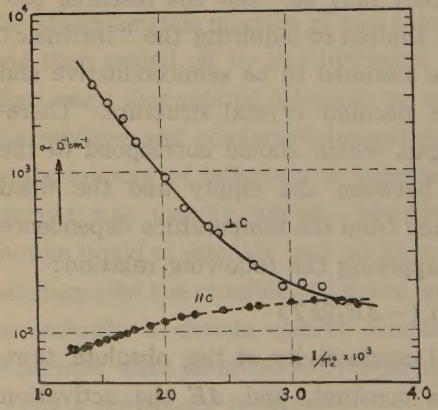

Fig. 1. Temperature dependence of the electrical conductivity of InTe.

Fig. 1 shows the temperature dependence of electrical conductivity of the compound. The abscissa indicates the reciprocal of absolute temperature as in the figures below. The specific conductivity is about 10^2 $(ohm\text{-}cm)^{-1}$ at room temperature. Conductivity as a function of temperature follows different courses according to the crystallographic directions to which current flows; the behavior of conductivity parallel to the c axis is metal-like with a negative temperature coefficient, while perpendicular to it is apparently semiconductive.

It should be remarked that the thermoelectric motive forces have shown positive sign for both directions measured with the value of 100~80μV./°C. at near room temperature. At least in that temperature, therefore, the major portions of charge carriers are not electrons but holes in crystal.

More research is necessary to explain the anisotropy of conductivity variance.

(2) **In_2Te_3.** H. Hahn and W. Klingler[4] prepared In_2Te_3 in the form of massive nugget. They found it to be of the sphalerite type in structure with $a_0=6.146\pm0.005$Å. by the X-ray powder method. They concluded that the one-third of equivalent sites for indium were vacant, and were distributed at random. There are 1.33 In_2Te_3 molecules in the unit cell.

As reported previously[7], our X-ray examination of the artificial single crystals revealed the existence of a superlattice with $a_0=18.40$Å, an about three-fold lattice length. The space group symmetry was determined as T_d^2-F$\bar{4}$3m and with the density of 5.78 ± 0.04 gr/cm^3 at 20°C., the cell contains 35.6 ± 0.5 In_2Te_3 molecules. In the crystals crystallized slowly by our procedures, indium atoms are presumably distributed regularly.

{111} cleavage surfaces of the crystal have shining metallic lustre. Colour and streak are lead-grey inclining to iron-black.

The results of the electrical conductivity measurement are shown in Fig. 2. In this case temperature dependence is typically of a semiconductor. From the slope of plotted data the

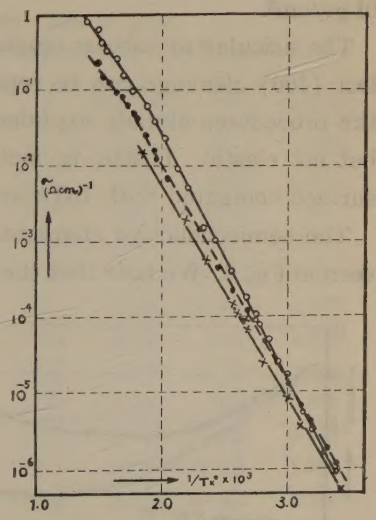

Fig. 2. Temperature dependence of the electrical conductivity of In_2Te_3.

average values of activation energy ΔE is calculated to be 1.15eV. between room temperature and 270°C. and 0.9eV. above 270°C.. With reference to the conclusion[11] deduced from the measurement of photoconductivity, the value 1.15eV. may indicate possibly the energy gap in this telluride. So, so far as our specimens are concerned, at room temperature the crystal is in the intrinsic conduction state as in an ideal ionic crystal, and this may be related to its strong tendency to grow with the exact stoichiometric proportion of constituent elements excluding almost all minor impurities.

Meanwhile, the crystal is piezoelectric.

(3) **$InTe_3$**. X-ray single crystal oscillation photographs were indexed on the basis of a monoclinic unit cell with a_0=19.7Å, b_0=4.37Å, c_0=12.8Å. and β=101°. Crystals are occasionally twinned on {100}, although not observed by the microscopic observation. The possible space group is either C_{2h}^3-C2/m, C_2^3-C2 or C_s^3-Cm. The unit cell contains 8.04 $InTe_3$ molecules calculating from the density of 6.08±0.-01 gr/cm³.

The acicular or tabular crystals elongated to the b axis with perfect {100} cleavage can be separated from the ingot prepared by the procedures already explained. Cleavage flakes are very flexible, but not elastic. Lustre is metallic, less splendent on the cleaved surface compared with InTe and In_2Te_3 crystals. Streak is grey.

The semiconductive characters of electrical conductivity may be seen in Fig. 3. We note that the σ *versus* $1/T$ curves (two typical cases are shown), although at lower temperature they take different courses according presumably to the difference in contents and sorts of impurities, become a single curve at higher temperature. Extraporating it over the high temperature range not depicted in the figure, we

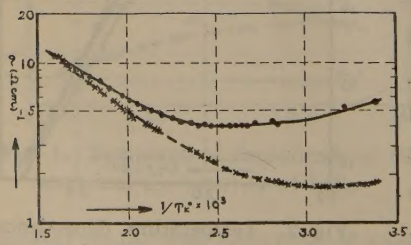

Fig. 3. Temperature dependence of the electrical conductivity of $InTe_3$.

have estimated the energy gap to be about 0.5eV.. Recently E. Mooser have obtained by a similar method the value 0.36eV.* with regard to his $InTe_3$ specimen.

II. *Indium selenides.* Two of indium selenides, InSe and In_2Se_3, were prepared. We know, according to W. Klemm and H.U. von Vogel[8], the melting points are $660\pm10°C$. for InSe and $890\pm10°C$. for In_2Se_3.

(1) InSe. Recently R.W. Damon and R.W. Redington[1] prepared InSe crystal by the same procedure as described here, and studied the optical and electrical properties.

By the X-ray single crystal oscillation photographs, the hexagonal symmetry was deduced, an orthohexagonal cell having been measured; 19.2Å., 33Å. and 4.00Å.. From these the hexagonal unit cell has the dimensions; $a_0=19.2\pm0.1$Å., $c_0=4.00\pm0.02$Å. and $c_0/a_0=0.208$. The X-ray powder diagram was taken by a Norelco spectrometer and indexed (Table 1).

Table 1. X-ray powder data of InSe.
Cu$K\alpha$, 40 KV., 13 mA. (Norelco). Hexagonal; $a_0=19.2$Å., $c_0=4.00$ Å.

I	*d*(meas.)	*hk,l*	*d*(calc.)	*I*	*d*(meas.)	*hk,l*	*d*(calc.)
W	8.36Å	20 0	8.32Å	W	1.80Å	40,2	1.80Å
S	4.16	40,0	4.16	VW	1.73	65,0	1.74
MSbr	3.38	21,1	3.38	VW	1.62	43,2	1.60
VW	3.14	42 0	3.14	VW	1.44	80,2	1.44
Wbr	3.05	22,1	3.07	VW	1.40	10 2,1	1.40
Wbr	2.96	51,0	2.99	W	1.388	12 0,0	1.387
VW	2.77	60,0	2.77	VW	1.353	90,2	1.358
Wbr	2.44	44,0	2.40	VW	1.263	10 4,1	1.264
Wbr	2.38	70,0	2.38	VW	1.197	88,0	1.201
VW	2.30	60,1	2.28	VW	1.187	14 0,0	1.188
VW	2.08	80,0	2.08	W	1.160	12 3,1	1.158
S	2.00	00,2	2.00	Wbr	1.154	10 3,2	1.153
VW	1.95	71,1	1.93	MSbr	1.140	12 0,2	1.140

* Private communication from E. Mooser.

The space group is decided to be D_6^6-$C6_32$. The density being 5.72 ± 0.05 g/cm^3 the unit cell contains 22.7 ± 0.4 InSe molecules. A chemical analysis has given the composition $In_{1.03}Se_{1.00}$ for the synthesized crystals.

{10$\bar{1}$0} cleavage fllakes elongated parallel to the c axis are easily separated from ingot. The crystal is somewhat flexible. Both colour and streak are blackish grey. Although the crystal has dull metallic lustre, a very thin flake is feebly transparent with a dark brownish hue.

Fig. 4 gives typical results of the conductivity measurements on InSe cleavages. The room temperature conductivity parallel to cleavage plane was measured to be $3\sim10\times10^{-5}$ (ohm-cm)$^{-1}$, which is of the same order as that of In_2Te_3 crystal. The variation of conductivity at and near room temperature is different, presumably dependent on the amount of impurities in each specimen. At the moderate high and highest temperature ranges, however, the curves become, as in the case of $InTe_3$ described above, straight and parallel to each other. We have noticed that a knick take place on each curve at about 265°C.. The values 1.15eV. and 2.24eV. were calculated for their activation energies at respective temperature ranges. R.W. Damon and R.W. Redington[1] obtained a somewhat different value for the activation energy (ΔE=0.97eV.) for the whole temperature range.

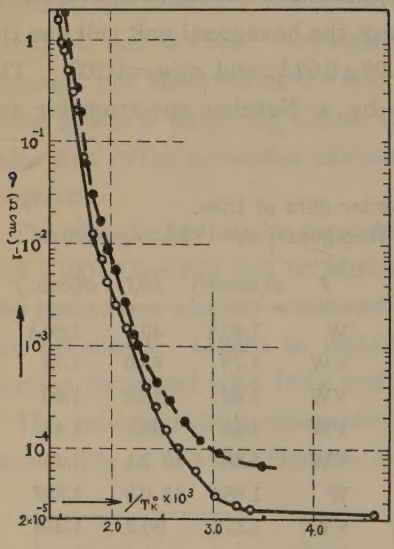

Fig. 4. Temperature dependence of the electrical conductivity of InSe.

According to H. Miyasawa who experimented with cleaved speci-

mens supplied by us, a maximum occurs in photoconductivity at the 1.25eV. absorption edge. This has led us to conclude that of the values deduced, 1.15eV. should be taken for the energy gap rather than 2.24eV.. The latter value may have been affected by the ionic conduction which might have taken place within the specimen.

(2) In_2Se_3. H. Hahn[2] reported that In_2Se_3 has a hexagonal unit cell with a_0=3.99Å., c_0=19.0Å. and c_0/a_0=4.76 containing 2 In_2Se_3 molecules. We have confirmed his result. The X-ray powder diagram (Table 2) taken by a Norelco spectrometer was indexed on the

Table 2. X-ray powder data of In_2Se_3.

Cu$K\alpha$, 25 KV., 18 mA. (Norelco). Hexagonal; a_0=4.00Å., c_0=19.24 Å.

I	d(meas.)	$hk.l$	d(calc.)	I	d(meas.)	$hk.l$	d(calc.)
MS	9.60Å	00,2	9.62Å	W	1.92Å	00,10	1.92Å
S	4.82	00,4	4.81	VW	1.86	11,4	1.85
MS	3.28	10,2	3.26	VW	1.82	10,9	1.82
MS	3.21	00,6	3.21	VW	1.71	20,2	1.70
W	3.07	10,3	3.05	VW	1.60	00,12	1.60
VW	2.82	10,4	2.81	W	1.37	00,14	1.37
W	2.58	10,5	2.57	VW	1.279	10,14	1.277
W	2.41	00,8	2.40	VW	1.158	30,0	1.155
W	2.37	10,6	2.35	W	1.137	30,3	1.136
MS	2.01	11,0	2.00	VW	1.107	30,5	1.106
VW	1.99	10,8	1.98				

basis of the hexagonal unit cell with a_0=4.00Å., c_0=19.24Å. and c_0/a_0=4.81. The space group symmetry was determined to be either D^4_{6h}-C6/mmc, C^4_{6v}-C6mc or D^4_{3h}-C$\bar{6}$2c. A chemical analysis showed the composition $In_{2.00}Se_{2.95}$ for the synthesized crystals.

The crystal of In_2Se_3 is somewhat flexible but not elastic with the very easy cleavage after {0001}. Colour and streak are blackish grey. Lustre is dull metallic. Generally In_2Se_3 and InSe crystals are very similar in appearance, although cleaved surfaces of InSe are rather more resinous. Nevertheless, our studies revealed as will

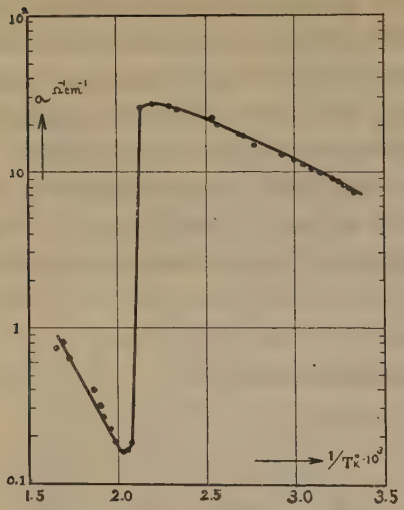

Fig. 5. Temperature dependence of the electrical conductivity of In_2Se_3.

curs in the latter case.

Corresponding to this a discontinuous change at the same temperature of the thermoelectric motive forces was measured, the temperature measured at the two sides of the specimen slip being averaged (Fig. 6).

These show the existence of a phase transition that occurs at the above mentioned temperature. It is remarked that a differential thermal analysis and a dilatometric measurement[12] which we have carried out be described below the remarkable difference in electrical properties between these two compounds.

As seen in Fig. 5, the magnitude of conductivity of In_2Se_3 ranges between 10~20 $(ohm\text{-}cm)^{-1}$ at room temperature. This is large compared with InSe. Moreover, an abrupt change in conductivity taking place at the temperature 200°C. is observable both by raising and lowering the temperature of measurement, although an appreciable supercooling oc-

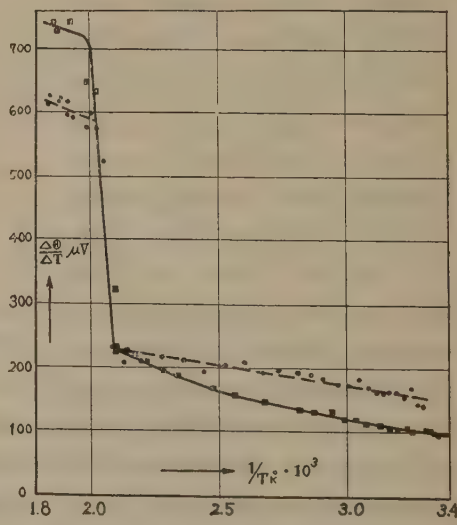

Fig. 6. Relation between thermoelectric motive force $\Delta\Theta/\Delta T$ and average temperature for two typical In_2Se_3 specimens.

on the same specimens have confirmed the result. Details including X-ray data concerning the phase transition will be later reported in another paper.

With the temperature coefficient of conductivity being positive (see Fig. 5), In_2Se_3 is, we conclude, no other than a semiconductor in both higher and lower temperature phases. The energy gaps could not be estimated for the above two phases of semiconductor because we were not certain whether we were here dealing with an intrinsic state or not.

Discussion of results

Indium selenides and tellurides studied here, in spite of their otherwise metallic appearance, have proved to be not metallic but semiconductive substances from their electrical examination. Accordingly it is said that the chemical bond in the compounds is not likely that of metal.

H. Krebs and W. Schottky[9] pointed out that the covalent bond is necessary to the occurrence of semiconductivity, and compared with a sp^3 hybridized electron whose eigen-function is essentially orientated towards one side of atom, *p*- or *d*-electron, its eigen-function being orientated towards two or even more directions of space, may easily resonate among those directions resulting to decrease the breadth of energy gap.

E. Mooser and W.B. Pearson[13] recently concluded from a survey of known various semiconductive compounds including In_2Te_3 that semiconductivity is the result of the presence in a solid of predominantly covalent bonds. According to them it is necessary that these bonds through the process of electron sharing, lead to completely filled *s* and *p* orbitals in valence shells of at least more electronegative constituent atom, which in most semiconductive compounds lies in IV to VII groups of the periodic table excluding the transition metals of these groups. The presence of empty metallic orbitals in some atoms of a compound, they say, does not destroy semi-

conductivity provided that these atoms are not bonded together. The covalent bonds must form continuous one-, two- or three-dimensional networks which run through the whole crystal.

So, it may be said, the crystal structure of compounds studied here have the networks of covalent bond from this point of view. In InTe which is isomorphous with TlSe, it is found, similarly to the case of TlSe interpreted by Mooser and Pearson, that each tellurium atom fills its s and p subshells receiving valence electrons from In atoms, and this situation may be seen by expressing its chemical formula as In^+ (In^{3+} Te_2^{2-}) from its crystal structure. The crystal consists of the $In^{3+}Te_2^{2-}$ chains where In^{3+} is tetrahedrally sur-

Table 3. Lattice types of III b metal mono-chalcogenides.

GaS[2]	GaSe[2]	GaTe[2]
hexagonal	hexagonal	monoclinic
$a_0=3.578$Å	$a_0=3.752$Å	$a_0=12.76$Å
$c_0=15.47$Å	$c_0=15.95$Å	$b_0=4.03$Å
$c_0/a_0=4.323$	$c_0/a_0=4.251$	$c_0=14.99$Å
		$\beta=103.9°$
InS	InSe	InTe[16]
not yet determined	hexagonal	tetragonal
	$a_0=19.2$Å	$a_0=8.42$ kX
	$c_0=4.00$Å	$c_0=7.12$ kX
	$c_0/a_0=0.208$	$c_0/a_0=0.84$
TlS[5]	TlSe[5]	TlTe[5]
tetragonal	tetragonal	not yet determined, but ascertained to be different from TlSe type.
$a_0=7.77$Å	$a_0=8.02$Å	
$c_0=6.79$Å	$c_0=7.00$Å	
$c_0/a_0=0.886$	$c_0/a_0=0.873$	

Compounds in an isomorphous relation are enclosed with same type of black lines.

rounded by four Te^{2-} atoms taking sp^3 hybridized bonds.

In other compounds, although determined here only their unit cell dimensions, such requirement for a semiconductor will be fulfilled in their crystal structures. This may give some clue to possible crystal structur.

Comparing the crystallographic data obtained, InSe and InTe crystals, however, have between them no isomorphous relation. This dissimilarity is also confirmed upon comparing their electrical conductivities with each other. As shown in Table 3, the monoselenides of III b metals are not isomorphous generally with their corresponding monotellurides. In the chalcogenides of gallium and thallium, it has been reported[2,5] that each of monoselenides has a structural counterpart in monosulphides. This relation can not be ascertained in indium chalcogenides because the crystal data of InS is not known yet. It is thought that the difference between the electronegativities of selenium and tellurium is critical on the properties of chemical bond with which these elements form the 1 : 1 compounds with gallium, indium and thallium.

Although InTe has a tetragonal lattice isomorphous with TlSe, InSe appears to have a different lattice from that of GaTe, which has a monoclinic layer lattice as determined by H. Hahn[2] and his colleagues.

Moreover, In_2Se_3, at least its lower temperature form, is also different from those of In_2Te_3 and other chalcogenides of III b metals as shown in Table 4. A comparison in lattice dimensions with the wurtzite type compounds, Al_2Se_3, Ga_2S_3, etc. might reveal that In_2Se_3 has a wurtzite-like superlattice structure. But the intensities of its X-ray powder diagram cannot be fully explained by this simple assumption.

In_2Se_3 is also conspicuously differing in its electrical properties from In_2Te_3. The former is rather conductive having the remarkable phase transition and the latter, on the other hand, is poorly conductive showing photoconductivity. So it is expected that their

Table 4. Lattice types of III b metal sesqui-chalcogenides.

Al_2S_3[17]	Al_2Se_3[15]	Al_2Te_3
[W] $a_0=3.70$Å $c_0=5.94$Å $c_0/a_0=1.61$	[W] $a_0=3.890$Å $c_0=6.30$Å $c_0/a_0=1.62$	not yet determined
Ga_2S_3[18]	Ga_2Se_3[18]	Ga_2Te_3[18]
α form [ZnS] $a_0=5.181$Å β form [W] $a_0=3.685$Å $c_0=6.028$Å $c_0/a_0=1.636$	[ZnS] $a_0=5.429$Å	[ZnS] $a_0=5.886$Å
In_2S_3[18]	In_2Se_3	In_2Te_3
α form [γ' Al_2O_3] $a_0=5.37$Å β form [γ Al_2O_3] $a_0=10.74$Å	Hexagonal $a_0=4.00$Å $c_0=19.24$Å $c_0/a_0=4.81$	[ZnS] $a_0=6.158$Å[18] or $a_0=18.40$Å superlattice type

[ ] shows the structure type of each compound, and
[W] means wurtzite structure.

electronic structures or their characters of covalent bond are much different from each other.

In In_2Te_3 with a sphalerite-like structure, valence electrons are in a sp^3 hybridized state. According to H. Krebs and W. Schottky's discussion, the sp^3 hybrid bond results larger breadth of the energy gap in semiconductive compounds. This explains the rather insulative property of In_2Te_3 having the breadth of energy gap 1.15eV.. On the other hand, because of its much higher conductivity, at least the lower temperature form of In_2Se_3 is thought to have a different type of covalent bond from that of sp^3 hybridization and probably the bond of p electron sharing. From this consideration it may be plausible that the crystal structure of In_2Se_3 is not of sphalerite, wurtzite or their superlattice type.

Acknowledgement

The author wishes to express his sincere gratitude to prof. T. Ito for his interest and guidance, and is indebted to Dr. H. Inuzuka for his kind encouragement throughout this work. The thanks are expressed to Dr. H. Miyasawa for his valuable informations and Messrs. Y. Uemura, J. Okada and M. Takabayashi for their valuable advice on the work.

REFERENCES

1) Damon, R.W. & R.W. Redington: Phys. Rev., **96**, 1498 (1954).
2) Hahn, H.: Angew. Chemie, **65**, 538 (1953).
3) Hahn, H. & W. Klingler: Z. anorg. Chem., **259**, 135 (1949).
4) Hahn, H. & W. Klingler: ibid., **260**, 97 (1949).
5) Hahn, H. & W. Klingler: ibid., **260**, 110 (1949).
6) Henisch, H.K. & M. Francois: Semiconducting Materials, London, 234 (1951).
7) Inuzuka, H. & S. Sugaike: Proc. Jap. Acad., **30**, 383 (1954).
8) Klemm, W. & H.U. von Vogel: Z. anorg. u. allgem. Chem., **219**, 45 (1934).
9) Krebs, H. & W. Schottky: Halbleiterprobleme I, (1954).
10) Lawson, W.D.: J. Appl. Phys., **22**, 1444 (1951).
11) Miyasawa, H. & S. Sugaike: J. Phys. Soc. Jap., **9**, 648 (1954).
12) Miyasawa, H. & S. Sugaike: ibid., **12**, 312 (1957).
13) Mooser, E. & W.B. Pearson: Phys. Rev., **101**, 1608 (1956).
14) Pauling, L.: The Nature of Chemical Bond, (1939).
15) Schneider, A. & G. Gattow: Z. anorg. u. allg. Chem., **277**, 49 (1954).
16) Schubert, K., E. Dorre & M. Kluge: Z. Metallkunde, **46**, 216 (1955).
17) Smithells, C.J.: Metals Reference Book, Vol. I, London, 211 (1955).
18) Structure Reports for (1949).

Manuscript received January 10, 1957.

Mineralogical Journal, Vol. 2, No. 2, pp. 78–89, June, 1957

THE INTERPRETATION OF X-RAY POWDER DIFFRACTION PATTERNS OF THE SZAIBELYITE–SUSSEXITE SERIES

Yoshio Takéuchi

Mineralogical Institute, University of Tokyo

Abstract

Because of felted or matted fibrous nature of crystals, the symmetry and lattice constants of szaibelyite had not been determined. However, with aid of information obtained from oscillation pattern and poor Weissenberg photographs of sussexite (manganese analogue of szaibelyite), the indexing of powder diffraction patterns of szaibelyite and sussexite was successfully carried out. The results established the orthorhombic symmetry of the szaibelyite—sussexite series. The lattice constants found from X-ray powder data are:

		a_0	b_0	c_0
szaibelyite	(Mg, Mn)HBO_3	10.34Å	12.45Å	3.21Å
sussexite	(Mn, Mg)HBO_3	10.61	12.65	3.30

The variation of the lattice constants with changing chemical composition for the szaibelyite—sussexite series is discussed together with possible space groups.

Introduction

Szaibelyite is a simple hydro-borate with the chemical formula (Mg, Mn)HBO_3. There had also been described two other minerals, camsellite and ascharite having the composition $MgHBO_3$, and the relation between these minerals had long been the object of discussion untill in 1939 Watanabe[13] suggested the identity of these minerals on the bases of X-ray data. Then, Schaller[6], as the result of careful examination of the problem, established the identity and discussed the possible isomorphous series of $MgHBO_3$—$MnHBO_3$. However, due to the fibrous nature of these crystals, their symmetry and lattice constants have not been determined.

In connection with our studies of magnesium borates, several

years ago, the writer found the identity period along the fibre axis of szaibelyite as about 3.2Å.. Although the value is slightly larger than the c-axes of the other magnesium borates then examined, e.g. warwickite, fluoborite etc.. it appears very likely that the structure of szaibelyite may also be built up in the similar way as we have found with these magnesium borates[10)11)12)], but the knowledge of the structure of szaibelyite is of special interest because of the part played by the hydrogen atom in the borate.

As a preliminary course of the structure analysis of szaibelyite, the determination of the lattice constants was undertaken. This had to be done by interpreting the powder diffraction pattern because it is hardly possible to obtain its single crystals.

Preliminary investigation

The samples of szaibelyite examined in this experiment were from Douglas Lake, B.C. which were originally named as camsellite. A specimen, whose diameter was about 0.1 mm., was seperated from the fibrous part of the matted sample and was used for X-ray work. It was found that the Laue photograph taken with the incident X-ray beam perpendicular to the fibre axis gave a rotation pattern instead of the usual Laue pattern, thus revealing that the specimen consists of exceedingly fine fibrous crystals and their a- and b-axes are randomly orientated around the c-axis, if we denote the fibre axis as c-axis. The identity period of the c-axis measured from the above photograph was about 3.2Å. Once the period of one axis is known, the indexing of powder patterns becomes considerably easy. Especially in this case, the powder lines whose Q-values $\left(Q=\frac{1}{d^2}=\frac{4\sin^2\theta}{\lambda^2}\right)$ are smaller than about 0 1 must be the reflections only from $(hk0)$ planes.

However, it was possible to obtain more easily useful information about the other axes because a small piece of specimen of sussexite (manganese analogue of szaibelyite) which gives nearly uniform

extinction between crossed nicols was successfuly seperated. Although the Laue photograph of the specimen shows a pattern similar to that of szaibelyite, Weissenberg photographs give very encouraging results as mentioned below.

If the specimen is consisted of fibrous crystals whose a- and b-axes are distributed at random around their common c-axis, the Weissenberg photograph taken around the c-axis will give the pattern consisting of parallel continuous lines. However, as expected from the optical observation mentioned above, the Weissenberg photograph of the specimen did not give continuous lines but three maxima for each reflection. This means the distribution of a- (and b-) axes of the constituent fibres has three maxima. From corresponding maxima of each line, accordingly, the reciprocal lattice plane h^* k^* 0 was constructed. As shown in Fig. 1, the reciprocal lattice thus

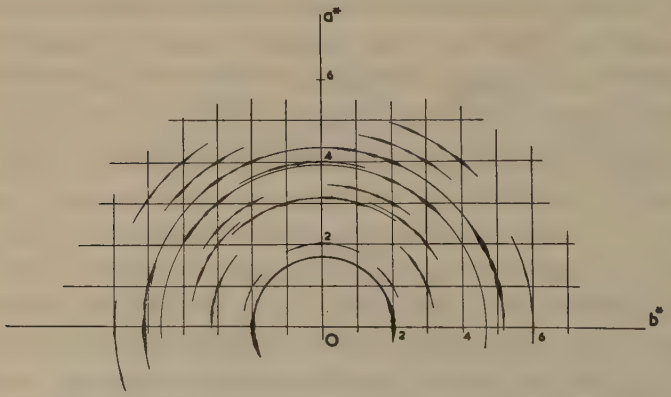

Fig. 1. Reciprocal layer of sussexite as constructed from the $hk0$ reflections which were recorded in the Weissenberg photograph.

obtained gives a rectangular symmetry with constants, a^*=0.145 and b^*=0.121 (λ=1.5418Å.). Due to the partially fibrous nature of the specimen, the pattern obtained in the Laue photograph simulates actually an oscillation pattern and is symmetric across the equator. Therefore, the results make it appear very likely that the

symmetry of sussexite is orthorhombic.

The results obtained in this section are summarized as follows.

sussexite		
	symmetry	very possibly orthorhombic
	lattice constants	a_0=10.6Å
		b_0=12.7
		c_0= 3.30
szaibelyite		
	symmetry	orthorhombic ?
	lattice constants	a_0 ?
		b_0 ?
		c_0=3.2Å

. The data of sussexite can be confirmed and refined by indexing its powder diffraction pattern from which the lattice constants of szaibelyite will also be derived.

Indexing of powder diffraction patterns

Sussexite

Reflections from powdered sussexite from Mine Hill, Sussex County N.J. were recorded on Norelco chart using Fe $K\alpha$ radiation. From 2θ values read on the chart, the interplaner distances and Q-values for each reflection were calculated. As previously discussed, it is clear that the peaks whose Q-values are smaller than 0.1 should be the reflections from ($hk0$) planes, so the indexing of these peaks was first tried. The Q-values of these peaks were compared with those calculated from the lattice constants derived from the Weissenberg photographs. Good agreement was obtained between the observed and calculated Q-values for the innermost two peaks and these were identified as 020 and 200. Intensities of these two reflections show also satisfactory agreement respectively with those of 020 and 200 observed in the Weissenberg photograph. The values of a^{*2} and b^{*2} which were obtained from Q-values of these two peaks

were successibly improved by indexing the peaks of the higher order.

Table 1. Interplaner spacings of sussexite. Observed and calculated Q-values are compared. $\Delta Q = Q\text{obs} - Q\text{calc}$.

d obs.	I	Q obs.	Q calc.	$\Delta Q \times 10^4$	hkl
6.290	100	.0253	.0250	+ 3	020
5.300	26	0356	0355	+ 1	200
4.070	10	0604	0605	− 1	220
3.919	24	0651	0652	− 1	130
3.408	36	0861	0862	− 1	310
3.306	48	0918	0918	0	230
3.087	44	1049	1049	0	320
2.811	27	1266	1273	− 7	201
2.713	71	1358	1355	+ 3	240
			1362	− 4	330
2.653	29	1420	1420	0	400
2.601	27	1479	1481	− 2	031
			1484	− 5	410
2.466	63	1644	1652	− 8	150
2.450	27	1666	1671	− 5	420
2.280	23	1924	1918	+ 6	250
			1918	+ 6	041
2.246	37	1982	1984	− 2	430
2.112	29	2242	2250	− 8	060
2.089	21	2291	2283	+ 8	510
			2280	+11	331
2.035	36	2414	2421	− 7	440
			2402	+12	411
2.013	39	2468	2470	− 2	520
1.786	24	3135	3138	− 3	501
			3152	−17	170
1.770	35	3192	3197	− 5	600
1.712	16	3412	3418	− 6	270
1.608	19	3867	3862	+ 5	370
1.530	26	4272	4277	− 5	222
1.506	25	4409	4414	− 5	710
1.492	21	4492	4484	+ 8	470
1.257	19	6329	6339	−10	481

The observed and calculated Q-values are compared in Table 1. The agreement is very satisfactory and, moreover, the intensities of

$hk0$ reflections correspond to those observed in the Weissenberg photograph. The lattice constants thus refined are:

$a^{*2}=0.00888$ $a_0=10.61\pm0.01$Å
$b^{*2}=0.00625$ $b_0=12.65\pm0.01$
$c^{*2}=0.09180$ $c_0=3.30\pm0.01$
$V=441.51$Å^3.

The result of the chemical analysis of sussexite by Bauer (Palache, 1928)[5] gives the chemical formula

$$(Mn_{0.75}, Mg_{0.25})HBO_3.$$

If there are eight formula units in the unit cell, the specific gravity of sussexite is calculated as 3.22.

Since it is hard to obtain pure sussexite, attention should be payed for intergrowth of other minute crystals, especially calcite and dolomite. In fact, the reflections with interplaner distance of 2.87Å. and 3.04Å. appeared in the powder lines of sussexite were identified, respectively, as the strongest reflections from dolomite and calcite.

Szaibelyite

For recording powder lines of szaibelyite by Norelco diffractometer, copper radiation was used. The specimen used was camsellite as stated previously.

The indexing of the diffraction peaks was carried out in the similar way as in the case of sussexite. The calculated and observed Q-values are compared in Table 2. It seems that the agreement of these Q-values are good enough to conclude that szaibelyite is isomorphous with sussexite and belongs to orthorhombic symmetry. This agrees with the observed straight extinction of camsellite[2]. The lattice constants obtained are:

$a^{*2}=0.00935$ $a_0=10.34\pm0.01$Å
$b^{*2}=0.00645$ $b_0=12.45\pm0.01$
$c^{*2}=0.09700$ $c_0=3.21\pm0.01$
$V=413.23$Å^3.

As the chemical formula can be expressed by

Table 2. Comparison of observed and calculated Q-values of szaibelyite (camsellite).

d obs.	I	Q obs.	Q calc.	$\Delta Q \times 10^4$	hkl
6.197	100	.0260	.0258	+ 2	020
5.165	51	0375	0374	+ 1	200
3.966	8	0636	0635	+ 1	220
3.847	19	0676	0675	+ 1	130
3.324	17	0905	0907	− 2	310
3.240	45	0952	0955	− 3	230
3.020	41	1096	1100	− 4	320
2.657	75	1416	1406	+10	240
			1422	− 6	330
2.586	30	1495	1496	− 1	400
2.533	40	1559	1551	+ 8	031
			1561	− 2	410
2.424	75	1702	1707	− 5	150
2.313	32	1869	1876	− 7	340
2.202	77	2062	2070	− 8	321
2.199	38	2068	2077	− 9	430
2.079	62	2314	2322	− 8	060
1.992	26	2520	2528	− 8	440
			2531	−11	411
1.967	11	2585	2583	+ 2	051
			2596	−11	520
1.932	11	2681	2677	+ 4	151
1.779	11	3160	3164	− 4	360
1.726	19	3357	3366	− 9	600
1.662	9	3621	3624	− 3	620
1.607	8	3873	3880	− 7	002
1.555	9	4136	4131	+ 5	071
			4134	+ 2	361
1.538	10	4228	4222	+ 6	180
1.510	13	4386	4398	−12	640
1.493	12	4486	4502	−16	280
1.474	13	4602	4594	+ 8	621
1.426	6	4919	4917	+ 2	631
1.377	8	5274	5286	−12	242
1.338	6	5586	5587	− 1	152
1.293	8	5981	5984	− 3	800
1.241	6	6493	6476	+17	522

$(Mg_{0.88}, Mn_{0.12})HBO_3$,

the calculated specific gravity is 2.75, eight chemical units being assumed in the cell.

Reflections of dolomite and chrysotile were identified in the powder lines. These lines are not listed in Table 2.

Magnesiosussexite

To confirm above results, the indexing of powder data of magnesiosussexite, which was originally described by Gruner[3], was also tried. Since the specimen was not available, the data obtained by Gruner was used.

The agreement between observed and calculated Q-values which are listed in Table 3 is reasonable. The lattice constants derived are:

Table 3. X-ray powder data of magnesiosussexite calculated from Gruner's observation. Calculated and observed Q-values are compared.

d obs.	I	Q obs.	Q calc.	$\Delta Q \times 10^4$	hkl
6.23	m	.0257	.0254	+ 3	020
2.67	m	1396	1394	+ 2	330
2.57	w	1520	1526	− 6	410
			1521	− 1	031
2.44	m	1684	1679	+ 5	150
2.22	w	2029	2027	+ 2	321
			2033	− 4	430
2.09	w	2285	2286	− 1	060
2.01	vw	2485	2476	+ 9	411
			2478	+ 7	440
1.930	vw	2684	2666	+18	421
1.745	vw	3284	3290	− 6	600
1.621	vw	3805	3800	+ 5	002
1.570	vw	4057	4059	− 2	361
			4062	− 5	071
1.507	w	4403	4420	−17	222
1.379	vw	5258	5262	− 4	402
1.341	vw	5562	5576	−14	600

$a^{*2}=0.00914$ $a_0=10.46\pm0.01$Å
$b^{*2}=0.00638$ $b_0=12.52\pm0.01$
$c^{*2}=0.09500$ $c_0=3.24\pm0.01$
$V=424.31$Å^3.

The calculated specific gravity is 2.91, eight chemical units of $(Mg_{0.69}, Mn_{0.31})HBO_3$ being assumed in the unit cell.

Szaibelyite—sussexite series

A diagram showing relation between the interplaner spacings of

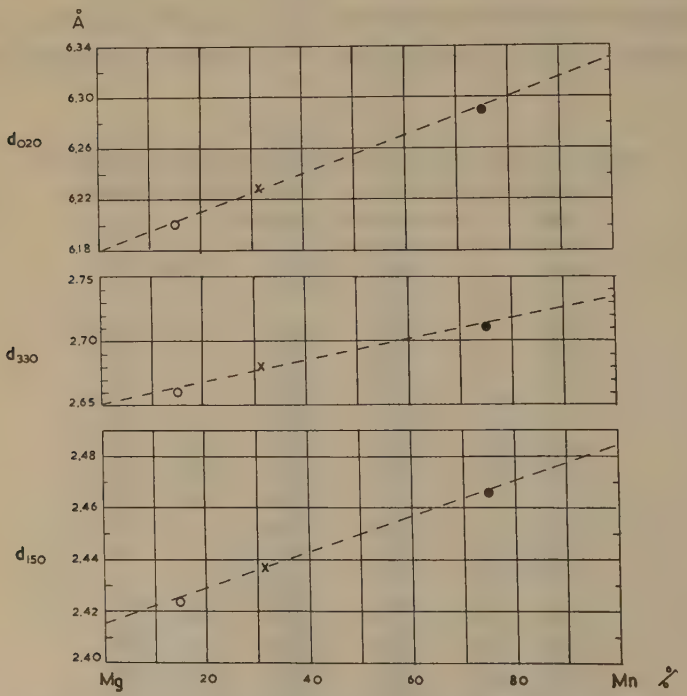

Fig. 2. Diagram showing relations between interplaner spacings of three strongest powder lines and component composition (mol percentage).

○ szaibelyite (camsellite) from Douglas Lake, B.C.
× magnesiosussexite.
● sussexite from Sussex Co., N.J.

three strongest powder diffraction lines and component composition (mol percentage) is shown in Fig 2. The plotted data are those shown in Tables 1, 2 and 3. The points corresponding to each composition lie approximately on a straight line. Although the diagram was obtained by using specimens of only three different compositions, it may provide means of deriving chemical composition from the interplaner distances if really complete series exists between the Mg and Mn end-members.

These three interplaner spacings of other available szaibelyites from different locality were also measured. They are listed in Table 4. Although chemical analysis has not been done, it seems, as seen in Table 4, that the specimen from Ta-huang-kon, Kuan-tien-hsien,

Table 4. Interplaner spacings of three strongest powder lines of szaibelyite from several localities.

Locality	d_{020}	d_{330}	d_{150} (Å)
Ta-huang-kon, Manchuria	6.18	2.651	2.418
Rézbánya, Hungary	6.21	2.659	2.425
Blind Mt., Nevada	6.20	2.660	2.425
Marin Co., California (camsellite)	6.22	2.660	2.427
Siberia, USSR (ascharite)*	6.18	2.67	2.43
Indersk, USSR (ascharite)*	?	2.690	2.451
Chicago Mine, Michigan (sussexite)**	?	2.74	2.46

* L.I. Shabynin (1955)[9]
** C.B. Slawson (1934)[8]

Manchuria is presumably the pure end-member, $MgHBO_3$. In fact, the observed interplaner spacings are in good agreement with the extrapolated values for the pure Mg component in the diagram shown in Fig 2. The extrapolated values are:

$$d_{020}=6.18\text{Å}$$
$$d_{330}=2.652$$
$$d_{150}=2.415.$$

In the original tables showing the chemical compositions of szaibelyite from Rézbánya, Hungary[7] and Blind Mt., Nevada[4] and camsel-

lite from Marin Co, California[1], MnO is not included. However, referring to the diagram shown in Fig. 2, the interplaner spacings of these minerals suggest that these are of composition similar to camsellite from Douglas Lake, B.C.. The interplaner spacings of sussexite from Chicago Mine, Michigan obtained by Slawson[8] show somewhat marked deviation from rest of data in Table 4, but the further investigation seems to be necessary with this specimen.

Some chemical analysis of szaibelyite indicate the existence of FeO in this mineral. However, due to difficulty of separation, it has not been decided upon if FeO is really the essential component of szaibelyite. To the case where iron replaces magnesium, the diagram shown in Fig. 2 will not be applicable.

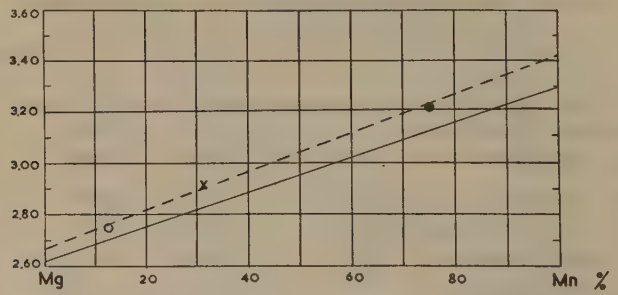

Fig. 3. Relation between specific gravity and component composition of the szaibelyite-sussexite series. The observed result obtained by Schaller[6] is indicated by solid line. Component composition is given by mol percentage.

The variation of calculated specific gravity with changing chemical composition is shown in Fig. 3. The values are slightly higher than measured values[6]. The extrapolated values are 2.68 for the Mg end-member and 3.42 for the Mn end-member, while Schaller's extrapolation gives 2.62 and 3.30 for the Mg and Mn end-member respectively[6].

Possible space groups

Negative result of piezo-effect suggests the holohedral symmetry

for szaibelyite. Observed extinctions of X-ray spectra are:

hkl	non
$hk0$	non
$h00$	$h=2n+1$
$0k0$	$k=2n+1$.

Due to multiplicity of powder lines, the extinctions of $0kl$ and $h0l$ are ambiguous. However, from above data, a conclusion can be drawn that plane group of $hk0$ is p_{gg}. This limits the possible space groups of szaibelyite to Pxym, where x and y are b- (or a-) or n-glide and should not be c-glide nor mirror plane.

As it is hardly possible to separate single crystals of these minerals, the above investigation will be of great help for the further steps of the structure analysis.

Acknowledgement

I am indebted to Professor Takeo Watanabe of the Geological Institute for his kind advice and furnishing materials, to Professor T. Ito and Dr. R. Sadanaga for helpful discussions.

REFERENCES

1) Eakle: Am. Min., **10**, 100 (1925).
2) Ellworth, H.V. and Eugene Poitevin: Trans. Roy. Soc. Canada, Sec. IV, Ser. III, **15**, 1 (1921).
3) Gruner, J.W.: Am. Min., **17**, 509 (1932).
4) Gillson and Shannon: Am. Min., **10**, 137 (1925).
5) Palache, C.: Am. Min., **13**, 323 (1928).
6) Schaller, W.T.: Am. Min., **27**, 467 (1942).
7) Stromeyer: Ak. Wien, Sitzber., **47**, 347 (1863).
8) Slawson, C.B.: Am. Min., **19**, 575 (1934).
9) Shabynin, L.I.: Dokl. Akad. Nauk SSSR, **101**, 937 (1955).
10) Takéuchi, Y., T. Ito and Takeo Watanabe: Acta Cryst., **3**, 98 (1950).
11) Takéuchi, Y.: Acta Cryst., **3**, 208 (1950).
12) Takéuchi, Y.: Acta Cryst., **5**, 574 (1952).
13) Watanabe, Takeo: Mineral. u. Pet. Mitteil., **50**, 454 (1939).

Manuscript received January 31, 1957.

Mineralogical Journal, Vol. 2, No. 2, pp. 90-102, June, 1957

THE ABSOLUTE STRUCTURE OF ULLMANITE, NiSbS

Yoshio Takéuchi

Mineralogical Institute, University of Tokyo

Abstract

The crystal of ullmanite from Sakhendorf, Siegerland has the lattice constant $a_0=5.881\pm0.002$Å.. Single crystal investigation confirmed the predicted space group T^4—$P2_13$ and the crystal structure was established by means of the two dimensional Fourier method. The bond distances found in ullmanite are:

Ni—Sb=2.57Å
Sb—S =2.40
Ni—S =2.34.

These results give the atomic radii for Ni 1.26Å., for Sb 1.32Å. and for S 1.08Å.. The radii of antimony and sulphur found in ullmanite are close to the Huggins' values.

Since the three fold axis of the crystal is polar, the determination of the absolute structure of the crystal was also carried out. With the aid of the anomalous X-ray scattering of Zn $K\alpha$ radiation by Ni atoms, correlation of the crystal structure of the crystal to the external form was made.

Introduction

Although it was as early as in 1930 that the study on the relation between the external form of a polar crystal and its structure was initiated by Coster, Knoll and Prins[4], it is to be regretted that the following development of the research had not been satisfactory. In fact, effort of producing further examples has never been made though technique has been developed of determing the absolute configuration of optically active compounds by means of X-ray anomalous scattering[1,2,12,14]. In spite of these circumstances, however, the problem is of vital importance to the understanding of the nature of the crystal, because a polar crystal provides us with the typical

example of directional changes in properties of the crystal, such as the degree of development of faces and electric conductivity, and on the study of the relation between the external properties of a polar crystal with its structure, we are to offer a key to the understanding of various properties of the crystal in terms of the atomic arrangement in its structure.

In view of the importance of the knowledge concerning the structure of a polar crystal with special reference to its external form, it is called "*absolute structure*" in the present paper, in order to distinguish it from the "*ordinary structure*" determined without reference to its external form. The term "*absolute structure*" is, therefore, applicable even to a crystal having mirror plane as far as it belongs to a polar class in contrast with the term "*absolute configuration*" which is categorically true only to optically active crystals lacking mirror planes.

As the examples of the determination of absolute structures, the minerals of the ullmanite group were examined and are described in the following. The members of the group are:

cobaltite	CoAsS,
gersdorffite	NiAsS, and
ullmanite	NiSbS,

but among these, cobaltite and gersdorffite were unfortunately found to be unsuited for the purpose. The X-ray diffraction pattern of the former suggested the presence of some kind of disorder in the structure prohibiting the straightforward analysis. On the other hand, though the X-ray powder diffraction pattern of the latter did not show such an anomaly, it is difficult to obtain its single crystals for morphological study. Therefore, ullmanite is the only material in this group suitable for the present investigation. To establish the structural type of this group, it is also fruitful to study the crystal structure of ullmanite, the details of the structural type being probably most clearly demonstrated in this species which contains Sb and S atoms whose size difference is larger than that be-

tween As and S.

In this study, the atomic parameters were first determined and then the absolute structure was investigated.

Lattice constant and space group

The lattice constant of ullmanite from Sakhendorf, Siegerland was measured on powder data recorded with a Norelco X-ray diffractometer and was found to be

$$a_0=5.881\pm0.002\text{Å}.$$

The space group determined from the Weissenberg photographs taken around the cube axis is T^4—$P2_13$, which agrees with the one reported previously by Ramsdell[13]. There are four molecules in the unit cell giving calculated specific gravity of 6.90 which compares well with the value of 6.793 deduced for the ideal composition[9].

The space group of cobaltite was also examined using a notable cube crystal which was kindly furnished by Dr. H.D. Wright of the Pennsylvania State University. The Weissenberg photographs of the crystal gave patterns similar to those of ullmanite except the appearance of odd order reflections from the cube faces (Plate I, Fig. 1). The presence of these reflections rules out the space groups T^4—$P2_13$ and T_h^6—$Pa3$ as was concluded by Peacock[11] from powder data. Moreover, intensities of (110), (011) and (101) reflections are not identical (To avoid the confusion due to the anomalous scattering of Cu radiation by Co atoms, Co radiation was used for this case). This result established that the symmetry of cobaltite is not exactly cubic as has long been suspected. Since it seems probable that the structure of cobaltite is essentially the same as ullmanite, the deviation from cubic symmetry may be explained either by twinning or by some kind of disorder. Beside the above specimen, cobaltite crystals from different localities were also examined with exactly the same results.

Determination of the atomic parameters

For recording *hk*0 intensities, copper radiation was used. The

intensity data were collected in multiple film sets of the Weissenberg photographs and each of the intensities was estimated visually with the aid of an intensity scale. As the structure of ullmanite is closely related to that of pyrites, a probable structure of ullmanite was derived by replacing iron atoms and S_2 groups in the FeS_2 structure respectively by nickel atoms and SbS groups and by adjusting their positions in reference to the theoretical atomic radii. Then the values of $F(hk0)$ were calculated.

Since the result of the calculation showed acceptable agreement between the calculated and the observed structure factors, the signs of the calculated ones were adopted for the observed amplitudes and the first Fourier projection $\rho(xy)$ was computed. In the projection, it was fouud that the nickel atom is considerably displaced from the conventional origin of the cell.

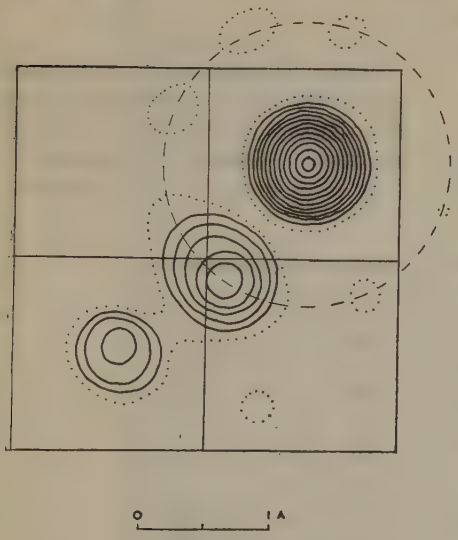

Fig. 2. The final electron-density projection on (001). The contours are drawn approximately at intervals of 5e.Å^{-2}, the dotted contour being the zero-electron line. The locations of diffraction ripples caused by antimony atom are indicated by dashed circle. A quarter of cell is shown.

Refinement of the structure was accomplished with the method of difference synthesis. The final electron density map is shown in Fig. 2. In this map, the electron density of the nickel atom gives the value of 29.5e/Å^{-2} at the center of the peak. However, in the Fourier projection which was obtained by subtracting the contribution of antimony atoms, its electron density was reduced to 27.7 e/Å^{-2} (Fig. 3).

For the final structure, the value of $R=\Sigma||F_0|-|F_c||\div\Sigma$

$|F_0|$ is 11.5%. Table 1 shows the agreement between observed and calculated values of the structure factors. The atomic scattering curves used for Sb and Ni atoms were those by Thomas-Fermi and for the sulphur atom, the Hartree curve was employed. They were modified by a temperature factor of $\exp(-B\sin^2\theta/\lambda^2)$ with 0.8Å^2 for the value of B. The atomic parameters found in the final structure are listed in Table 2. (Refer to Plate II, Fig. 4.)

For the estimation of errors in the coordinates, Cruick-

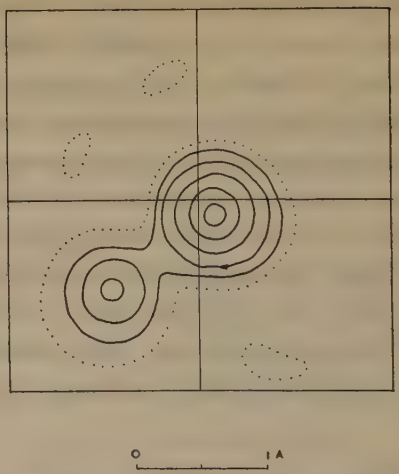

Fig. 3. The electron-density projection based upon F_0 ($hk0$) from which the contribution of antimony atom is subtracted. Contours at intervals of 5e.Å^{-2}. A quarter of cell is shown.

Table 1. Comparison of observed and calculated structure factors for ullmanite.

$hk0$	F_0	F_c	$hk0$	F_0	F_c
110	14.6	13.5	250	20.3	−21.5
120	23.8	25.0	260	5.7	− 6.7
130	13.6	−13.3	270	16.6	−17.6
140	5.5	5.9	310	6.6	− 6.6
150	9.8	− 9.4	320	13.0	11.3
160	7.3	− 4.6	330	12.7	16.3
170	8.5	7.4	340	3.7	− 6.5
200	20.1	−19.0	350	8.2	11.0
210	32.7	33.9	360	15.7	−14.7
220	18.4	−17.2	400	26.8	−24.1
230	27.7	28.8	410	0	0.3
240	11.7	−10.9	420	9.3	10.7

Fig. 1. Zero layer Weissenberg photograph of cobaltite around cube edge. The odd order reflections from the cube face are indicated. The photograph was taken by using cobalt radiation.

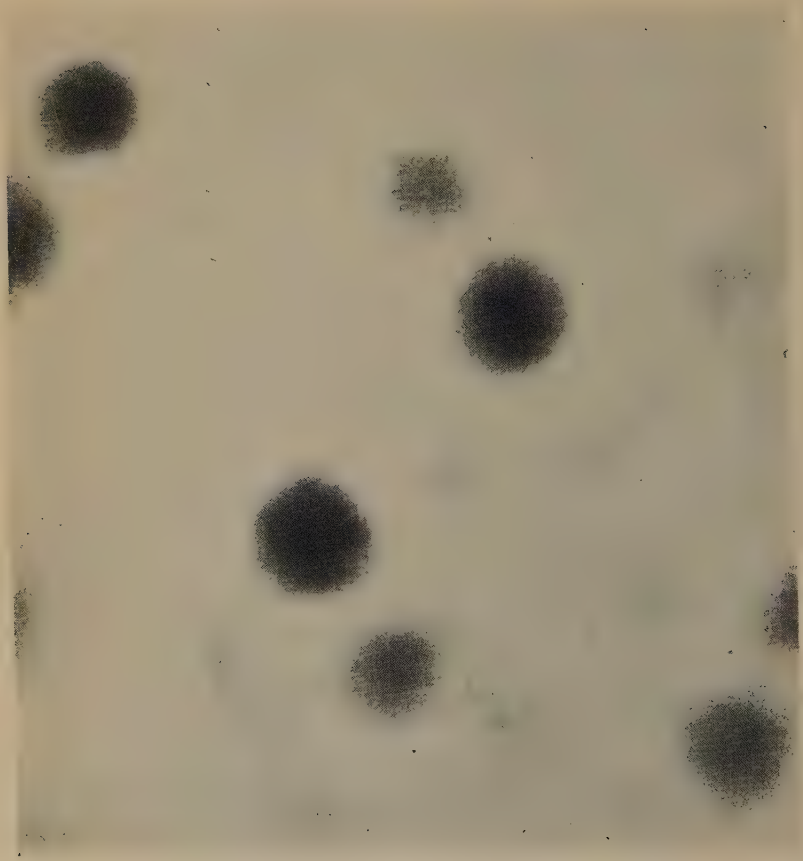

Fig. 4. Fourier projection $\rho(xy)$ of ullmanite, produced by Huggins mask. Sulphur atoms are migrated in the back ground.

$hk0$	F_0	F_c	$hk0$	F_0	F_c
430	0	1.0	600	4.2	− 5.0
440	33.8	36.0	610	17.0	−17.5
450	0	2.1	620	5.0	− 6.3
460	6.2	6.2	630	17.5	−17.8
510	15.6	−17.1	640	5.5	− 6.7
520	9.0	− 8.3	710	9.3	11.6
530	3.7	3.0	720	10.6	−13.6
540	3.3	4.3			
550	0	2.0			

Table 2. Coordinates of atoms.

Atom	x	y	z
Ni	−0.024	−0.024	−0.024
Sb	0.375	0.125	−0.125
S	0.390	0.390	0.390

shank's method[5] was applied since the projection of the structure has no overlapping of atoms, and the evaluated standard deviation, $\sigma(r)=\sqrt{2}\,\sigma(x)$, for each atom is given below.

Standard deviation	Estimated error
$\sigma(r)_{Sb}$	0.002Å
$\sigma(r)_{Ni}$	0.005
$\sigma(r)_{S}$	0.012

The errors caused by finite-series termination was also examined with result of maximum deviation $\Delta x=|x_{obs.}-x_{calc.}|$ of 0.020 for the sulphur atoms. These results seem to suggest that no bond length carries the error exceeding ±0.03Å..

Description of the structure

Fig. 5 shows the structure of ullmanite projected on to (001) and the structure is compared with the structure of pyrites in Fig. 6. The displacements of each atom in ullmanite from the corresponding

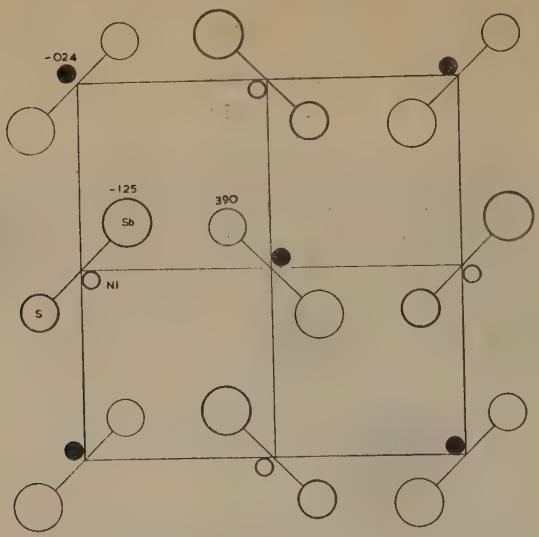

Fig. 5. Structure of ullmanite projected on (001). Solid and open small circles are nickel atoms whose z parameters are close to 0 and $\frac{1}{2}$ respectively.

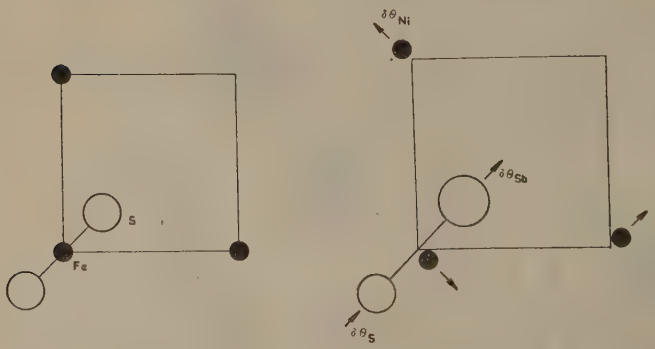

Fig. 6. Comparison of the quarter cells of pyrites and ullmanite structure. Origines are at the upper left corners. Only one of the S_2 and SbS groups is shown for pyrites and ullmanite.

position in the pyrite structure are as follows:

$$\delta\Theta_{Ni} = -14.4°,$$
$$\delta\Theta_{Sb} = -\ 7.0°, \quad \text{and}$$
$$\delta\Theta_{S} = -\ 2.4°.$$

Thus, the symmetry of the lowest cubic class of ullmanite is charac-

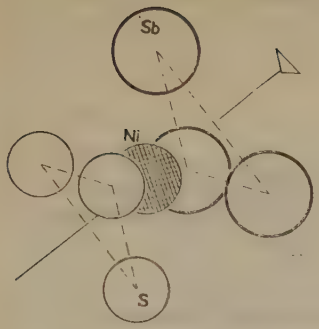

Fig. 7. Configuration of antimony and sulphur atoms about nickel atom in ullmanite.

terized by the substitution of the S_2 group in pyrites by the group SbS resulting a considerable shifting of Ni atom along the body diagonal direction of the cube. The nickel atom is surrounded by six neighbours, consisting of three antimony and three sulphur atoms as shown in Fig. 7. The interatomic distances between atoms in contact are:

$$\text{Ni—Sb}=2.57\pm0.03\,\text{Å.},$$
$$\text{Ni—S}\ =2.34\pm0.03\,\text{Å.},\ \text{and}$$
$$\text{Sb—S}\ =2.40\pm0.03\,\text{A}..$$

These values agree with the sum of the atomic radii given in the first column of Table 3 in which the values are compared with the radii of Sb and S found in gudmandite FeSbS[3] and also Huggins'

Table 3 Atomic radii of Ni, Sb and S.

	Radii computed from parameters of ullmanite	Huggins' tetrahedral radii	Radii found in gudmundite
Ni	1.26 Å	1.30 Å	
Sb	1.32	1.36	1.47 Å
S	1.08	1.04	1.13

tetrahedral radii[6]. The radii found in ullmanite show approximate agreement with those of Huggins' tetrahedral radii and considerably smaller than those of gudmandite It appears that the radius of S increases with the decrease in the symmetry of the minerals relating to ullmanite and gudmandite. This is conveniently discussed as follows.

increasing radius of S ⟶

		ullmanite NiSbS, 1.08			
	pyrites FeS_2, 1.07*		marcasite FeS_2, 1.11		
				gudmandite FeSbS, 1.13	↑ increasing radii of metal atom
Space group	T_h^6	T^4	V_h^{12}	C_{2h}^5	

Numerical numbers indicate the radius of the sulphur atom (Å).
* After Parker and Whitehouse[10].

Above relation also indicate the variation of the structural type by atomic radius of metal atom.

Non bonded distances found in ullmanite are given below.

Atom	Neighbour	Distance
Ni	Ni	4.16 Å
	Sb	3.59
	S	4.21
Sb	Sb	3.60
	S	3.41
S	S	3.61

Determination of the absolute structure

The ordinary external form of ullmanite is a cube, sometimes with pyritohedral striations. The occurrence of tetrahedral forms in this crystal was reported by Miers[8]. The combination of tetrahedral and pyritohedral symmetry means that the crystals should be referred to the lowest symmetry in the cubic classes. For the crystals, hkl, $\bar{h}kl$, $h\bar{k}\bar{l}$, $\bar{h}k\bar{l}$ are equivalent by symmetry but they are not equivalent with $\bar{h}\bar{k}\bar{l}$, $hk\bar{l}$, $\bar{h}kl$ and $h\bar{k}l$. If we look the crystal along the three fold axis of the crystal, the difference can be seen in the display of the striation on the cube (Fig. 8). While, in terms of its structure, the difference can be interpreted according to the differ-

ence in sequence of atoms along the body diagonal axis as shown in Fig. 9.

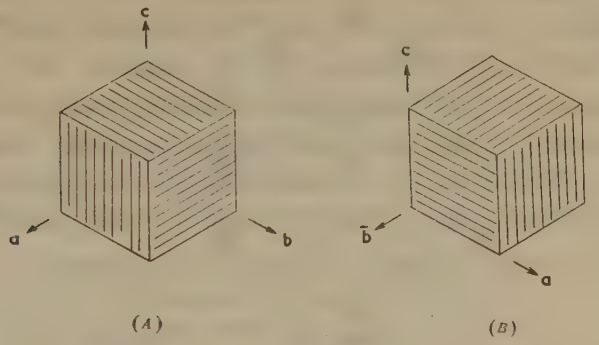

Fig. 8. External form of ullmanite seeing from [111] (A) and [$\bar{1}\bar{1}1$] (B) directions.

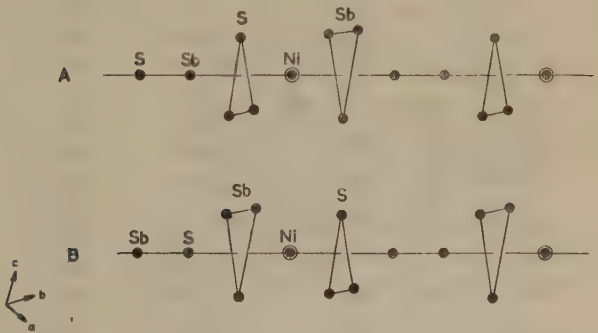

Fig. 9. The atomic arrangement on the three fold axis. Structure A corresponds to the structure based on the coordinates shown in Table 2. Structure B is the inverse structure of A, and it can be obtained by changing the signs of one of the coordinates in Table 2.

If the incident X-rays are of a wave length a little shorter than the absorption edge of the K electrons of the nickel atom, it will give rise to the difference in intensity between I_{hkl} and $I_{\bar{h}\bar{k}\bar{l}}$ as the result of the anomalous scattering of the X-rays by the atom.

This situation makes it possible to distinguish the structure A and B in Fig. 9 for a given coordinate system as shown in Fig. 8.

As the absorption edge of the K electrons of nickel is 1.484 Å., Zn $K\alpha$ radiation (λ=1.433 Å.) was used for the determination of the absolute structure of ullmanite. For this radiation $\Delta f'=-3.2$ and the imaginary part of the anomalous scattering becomes $\Delta f''=3.4$[7]).

The intensities which were recorded on oscillation photographs around the c-axis were first estimated visually and then measured with a microphotometer. They are listed in Table 4 together with

Table 4. Intensities of Oscillation photographs around the c-axis of ullmanite.

$h\ k\ l$	Observed intensities		Calculated intensities	
	hkl	$\bar{h}\bar{k}\bar{l}$	hkl	$\bar{h}\bar{k}\bar{l}$
1 1 1	>		192	64
1 3 1	?		929	818
1 5 1	<		528	614
2 1 1	?		64	69
2 3 1	>		482	372
2 5 1	>		453	296
3 1 1	?		940	828
3 3 1	>		114	28
3 5 1	>		197	103
4 1 1	?		197	201
4 3 1	?		181	181
4 5 1	?		46	40
5 1 1	?		530	618
5 3 1	<		65	137
5 5 1	>		171	109
1 4 2	<		555	731

the calculated intensities based upon the atomic coordinates listed in Table 2. The intensity differences were coufirmed by comparing them with the intensities on the oscillation photographs taken by Cu $K\alpha$ radiation. The conformity of the observed and calculated intensity inequalities suggest structure A, which is shown in Fig. 9, as the correct one. The projections of the absolute structure

which are looked from [111] and [$\bar{1}\bar{1}\bar{1}$] directions are compared in Fig. 10.

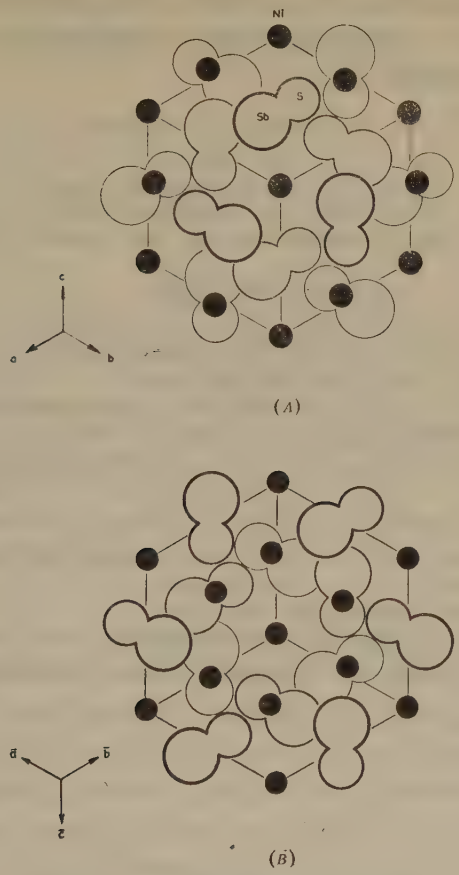

Fig. 10. The projections of the absolute structure of ullmanite from [111] (A) and [$\bar{1}\bar{1}\bar{1}$] (B) directions.

Acknowledgements

I am greatly indebted to Professor T. Ito and Dr. R. Sadanaga for helpful discussions and guidance. Special acknowledgement is due to Dr. H. Inuzuka, Tokyo Shibaura Electric Co., for excellent

technical help of preparing specimens for the determination of the absolute structure.

Thanks are also due to Professor Y. Saito, Osaka City University, for his critical reading of the paper, and to Dr. K. Sakurai for furnishing materials.

References

1) Bijvoet, J.M.: Proc. Acad. Sci. Amsterdam, **B 52**, 313 (1949).
2) Bijvoet, J.M., A.F. Peerdman and A.J. van Bommel: Nature, **163**, 271 (1951).
3) Buerger, M.J.: Z. Krist., **101**, 290 (1939).
4) Coster, D., K.S. Knoll and J.A. Prins: Z. Phys., **63**, 345 (1930).
5) Cruickshank, D.W.J.: Acta Cryst., **2**, 65 (1949).
6) Huggins M.L.: Phys. Rev., **28**, 1086 (1926).
7) James, R.W.: The Crystalline State II, Appendix III, (1948).
8) Miers, H.A.: Min. Mag., **9**, 211 (1891).
9) Palache, C., H. Berman and C. Frondel: The System of Mineralogy I, 301 (1946).
10) Parker, H.M. and W. Whitehouse: Phil. Mag., **7**, 14, 939 (1932).
11) Peacock, M.A. and W.G. Henry: Univ. Toronto Studies, Geol. Ser., No. 52, 71 (1948).
12) Peterson, S.W.: Nature, **176**, 395 (1955).
13) Ramsdell, L.S.: Am. Miner., **10**, 281 (1925).
14) Saito, Y., K. Nakatsu, M. Shiro and H. Kuroya: Acta Cryst., **8**, 729 (1955).

Manuscript received March 31, 1957.

Mineralogical Journal, Vol. 2, No. 2, pp. 103-113, June, 1957

NACRITE-BEARING KAOLIN CLAY FROM THE KASUGA MINE, KAGOSHIMA PREFECTURE, JAPAN*

Masayuki Tokunaga

*Geological Institute, University of Tokyo***

Abstract

Hypogene kaolin clay occurs in epithermal gold ore deposit of the Kasuga mine, as gangue mineral of vein and hydrothermal alteration product of wall rocks. They were examined under the microscope and by the X-ray powder method, and were also subjected to differential thermal analysis.

From the results of the studies, it is concluded that hypogene kaolin clay from the Kasuga mine is composed of nacrite, dickite and kaolinite. Some characteristic features in the occurrence of these minerals are described.

Introduction

Nacrite is the rarest mineral among the kaolin group. In 1949, Iwai and others[6] described the occurrence of nacrite and mixture of nacrite and dickite from the Yonago mine. In 1951, the writer found nacrite-bearing kaolin clay, in course of his study on the geology and ore deposits of the Kasuga mine, Kagoshima Prefecture, Southern Kyushu, Japan. The general description of the ore deposit and occurrence of nacrite-bearing kaolin clay was given in his previous reports[14][15]. Nacrite bearing kaolin clay was found in hydrothermally altered parts of the wall rocks and also as gangue mineral in epithermal gold-quartz veins.

In this paper the result of mineralogical investigation on the

---

* Read at the meeting of the Geological Society of Japan on April 5, 1953.

** Present address: Geological and Mineralogical Institute, Tokyo University of Education.

nacrite-bearing kaolin clay and characteristic features of occurrence of these minerals, together with the outline of the geology and the ore deposits are given.

Outline of the geology and ore deposits

The Kasuga mine* is located about 6 km. west of Makurazaki city, Kagoshima Prefecture, southwestern end of the Kyushu island (Fig. 1).

The gold ores of the Kasuga mine occur in numerous fissure-filling veins of the net-work type, in silicified propylitic tuff, tuff-breccia and propylite of the Tertiary. The hydrothermal solutions by which the wall rocks were silicified produced many other alteration effects in wall rock resulting in an interesting zonal arrangement of the mineral assemblages as given below.

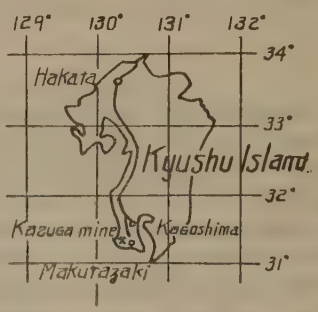

Fig. 1. Location map of the Kasuga mine.

(1) Horizontal zoning from inner zone to outer, silicified rock—dickite zone—limonite and kaolinite zone—kaolinite zone—original rock (propylite).

(2) Vertical zoning in the central area, from upper zone to lower, silicified rock—alunite zone.

Each altered zone changes gradually with conformable boundaries. The mineral assemblage in each altered zone is shown in Fig. 2.

Kaolin minerals are the chief constituents of hydrothermal alteration products in every zone, but each zone is characterized by specific kaolin mineral. Nacrite, dickite and kaolinite are found successively in successive altered zones from inner zone to outer, and the succession is in accord with that of the temperature range of stability

* 鹿児島県枕崎市春日鉱山

of those kaolin minerals.

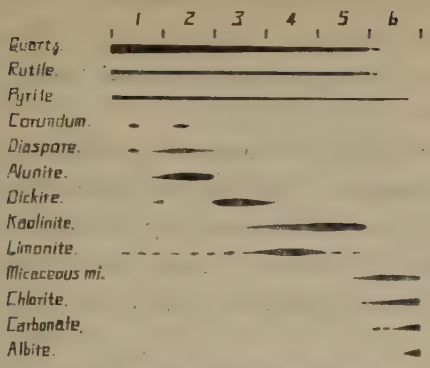

Fig. 2. The mineral assemblage in each altered zone.
1: Silicified rock. 2: Alunite zone. 3: Dickite zone. 4: Limonite and kaolinite zone. 5: Kaolinite zone. 6: Original rock.

Many fissures in various directions were observed in silicified rock. The major gold deposits form a zone consisting of net-work veins, which run longitudinally through the silicified area. The metallic minerals occur in these veins, and are also disseminated in silicified rock. In some cases fissures are also filled up with white clay which consists mainly of nacrite and fragments of silicified rock.

The ore minerals are native gold, luzonite, enargite and pyrite, and gangue minerals are quartz and nacrite-bearing kaolin clay.

The fissures formed after hypogene mineralization are also seen traversing silicified rocks, and are filled with supergene hydrated halloysite and montmorillonite. Among them, montmorillonite-bearing fissures yield high-grade gold ore enriched by supergene processes.

Occurrence of kaolin minerals

Two kinds of occurrence of nacrite-bearing kaolin clay are recognized,

(1) as white fissure clay that fills up fissures in silicified rock, associated with quartz, enargite and pyrite;

(2) and as chief constituents of hydrothermal altered zone around the silicified rock, associated with quartz, rutile, limonite after pyrite, and other secondary minerals.

In the first case, white fissure clay consists of abundant nacrite

and lesser amounts of dickite. They form generally fine aggregates which is liable to crumble in dry state at room temperature. The individual crystals show irregular, rounded, or flaky shape, $2\times3\mu$. in size. Therefore discrimination of each species under the microscope is quite impossible.

In the second case, the kaolin minerals are composed of dickite, kaolinite and a small amount of nacrite. The dickite, generally, occurs replacing the phenocrysts of original rocks, and is coarse-grained as shown in Fig. 3a (Plate I). Between crossed nicols it is revealed to be fan-shaped or bunchlike aggregates with a low birefringence.

The dickite found in small pocket in quartz aggregate, is in the form of six sided flakes, $5\times3\mu$. in dimensions (Plate 1, Fig. 3b), and form radiating aggregates up to $10\times15\mu$. in diameter. It is light brown or colourless under the microscope.

The kaolinite replaces the feldspar phenocrysts of original rocks and forms fine grained aggregates or vermicular form 10μ. in diameter. Even between crossed nicols it is difficult to discriminate individual particles. The kaolinite is colourless, and has a very low birefringence.

Differential thermal analysis

The thermograms were made with conventional differential thermal analysis apparatus arranged by T. Sudo and others[13]. The heating rate was approximately 10°C. per minute. The analyses have been carried on many specimens, but only representative curves are present, as shown in Fig. 4.

The interpretations of the thermograms are as follows:

(1) White fissure clay (No. 1, 2)

Specimen No. 1 is the crude specimen of vein-stuff in fissures.

Specimen No. 2 is a pure one refined from specimen No. 1 by elutriation method.

These specimens show a characteristic thermogram with a peculiar

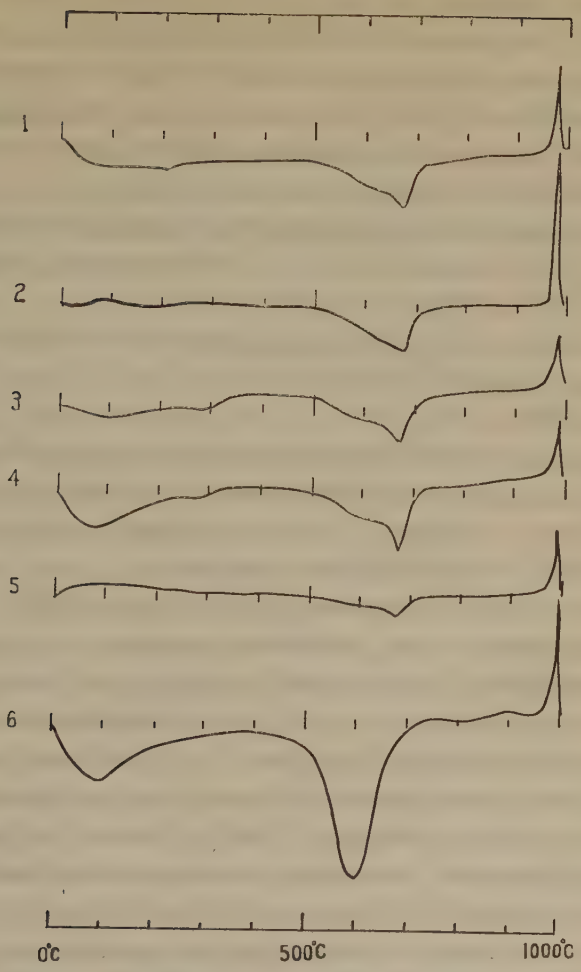

Fig. 4. Thermogram for kaolin minerals from the Kasuga mine.
1, 2: White fissure clay (nacrite).
3, 4, 5: Clay of the dickite zone (dickite).
6: Clay of the kaolinite zone (kaolinite).

broad endothermic peak at 675°C., the bend by decomposition beginning at about 500°C., and the sharp exothermic peak at 970°C..

These peak temperatures accord well with those given in literatures[4)10)] and from these features they may be assumed to be nacrite.

In most specimens nacrite is usually intimately associated with dickite[7)], and the obtained D.T.A. curves for nacrite usually overlap with those of dickite. It is therefore difficult to determine the presence of nacrite by the thermal method alone.

The small endotherm and irregularities in thermal curves between 100°~200°C. are supposed to be due to the impurities contained.

(2) Clay of the dickite zone (No. 3, 4, 5)

Crude specimens No. 3 and 4 are collected individually from the dickite zone around the silicified rock, and No. 5 is an elutriated specimen of No. 3.

The thermograms of these specimens show two peaks, one being a broad endothermic peak at 670°~680°C., and the other a sharp exothermic one at 980°~990°C., and are essentially similar to those of No. 1 and 2 with the following exceptions:

1. the bending of endothermic curve at about 560°C.;
2. abrupt turning of the endothermic peak; and
3. a considerably larger amount of endotherm between 100°~200°C.. From these features, the mixtures of large amounts of dickite and less of nacrite may be assumed. The shapes of the curves are in accord with those given in the literature on the subject.

Compared, however, with the artificial mixture of nacrite and dickite in literature[10)], the broad and assymmetric shape of the endothermic peak at 670°C. may be inferred to be an indication of the presence of nacrite. The relatively intensive endotherm between 100°~200°C. is supposed to be an indication of the presence of halloysite, and the small endotherm between 290°~300°C., of limonite.

(3) Clay of the kaolinite zone.

Crude specimen No. 6 is the clay from the kaolinite zone.

The curve consists mainly of three peaks; the conspicuous endothermic peak between 100° and 200°C., the high endothermic peak with a symmetrical form at about 600°C. and the sharp exothermic

peak at 990°C.. Although the latter two peaks have the proper ratio of intensities for those of kaolinite, the conspicuous endothermic peak between 100°~200°C. indicates the presence of halloysite or the irregular stacking of kaolinite unit layers. There are a slight endothermic peak at 800°C. and exothermic one at 900°C. which may be inferred to indicate the presence of montmorillonite group minerals. The slight endothermic peak at 300°C. is probably caused by a trace of limonite.

X-ray examination

X-ray powder diagrams were made with filtered Cu $K\alpha$ radiation using Philips Geiger-counter X-ray spectrometer. The calibration was based on reflection of quartz impurity and spacings of quartz are obtained from Brindley's data[1].

The interplaner spacings and the intensities of reflections are listed in Table 1 and are schematically illustrated in Fig. 5 comparing with the previous data[1,2,3,6,9,10]. The lines which were recorded but are probably due to impurities are listed at the bottom of each column of Table 1.

Samples 1 and 2 in Table 1 and Fig. 5 belong to the white fissure clays. The relatively strong intensity of the line of 2.39Å and the feature of triple lines around it, both characteristic for 1 and 2, are inferred to indicate the presence of nacrite. But the several lines between 4.5 and 3.5Å. which are absent in the previous data for nacrite may be those of dickite, and/or kaolinite.

Sample 3 belongs to the clay of the dickite zone. Its powder lines are conformable to those of dickite, with the characteristic quadruple lines around the 2.39Å. line and several lines between 4.5 and 3.9Å..

Sample 4 belongs to the clay of the kaolinite zone. Its powder lines agree with those for kaolinite except some weak lines which are absent and those which are probably due to impurities.

Table 1. X-ray powder lines for the kaolin minerals from the Kasuga mine.

	1		2		3		4	
	d (Å)	*I*	*d* (Å)	*I*	*d* (Å)	*I*	*d* (Å)	*I*
	7.2	77	7.2	100	7.2	100	7.2	100
	4.43	6	4.44	4	4.46	5.4	4.45	4
	4.36	6.3	4.37	3.3	4.39	6.9	4.39	4.6
	4.26	6.7	4.26	6.6	4.28	23		
	4.12	9.3	4.11	6.7	4.14	7.7	4.17	4.0
	3.96	10	3.97	6.0	3.99	3.1	3.98	2.6
	3.78	12	3.80	12	3.82	3.8		
	3.58	100	3.59	93	3.60	64	3.59	80
	3.43	4.7	3.43	4.6			3.43	1.3
			3.26	1.3				
			3.10	1.3				
	2.93	2.6	2.94	1.3				
	2.78	4	2.79	2.7				
	2.56	4	2.56	4	2.57	3.1	2.56	20
	2.52	6	2.52	6	2.51	3.1	2.53	26
	2.50	**4.6**	**2.50**	**5.3**				
	2.38	**40**	**2.39**	**21**	2.39	5.8		
	2.32	**10.6**	**2.32**	**16**	2.33	10	2.33	4.1
							1.94	4.3
					1.82	8.4	1.84	1.3
	1.78	18	1.79	10	1.79	3.1	1.79	2.4
					1.66	2.3		
	1.64	10	1.65	7.2	1.65	3.1	1.65	2.0
	1.55	4.7	1.55	3.3	1.55	1.5		
	1.48	2.6	1.48	3.3	1.48	3.8		
	1.43	4.7	1.43	3.3				
			1.42	2.0				
					1.38	2.3		
	1.37	2.0			1.37	4.6		
Impurities	3.33	10.6	3.33	1.8	3.34	92	3.35	4.0
	2.45	1.3			2.46	6.1	2.40	5.3
					2.29	3.8	2.29	4.0
					2.24	3.7		
					2.13	5.4		
	1.97	6.6	1.97	6	1.98	6.1	1.98	20
					1.67	1.5		
					1.54	6.1		

1, 2: White fissure clay (nacrite+dickite).
3: Clay of the dickite zone (dickite).
4: Clay of the kaolinite zone (kaolinite).
Bold style: Characteristic triple lines for nacrite.

Fig. 5. Schematic representation of X-ray powder photographs of kaolin minerals from the Kasuga mine together with some data previously published.

N1: Data for nacrite by Gruner.
N2: ditto by Ross & Kerr.
N3, N4: ditto by Nagelschmidt.
N5: ditto from Am. Petroleum Inst..
N6: ditto by Brindley.
N7: ditto by Claringbull.
N8, N9, N10: ditto by Iwai, Takeshi and Ossaka.
D1: Data for dickite by Brindley.
1, 2, 3 and 4: Present data for the clay minerals from the Kasuga mine. Numbers refer to Table 1.

Conclusion

From all the analyses by various methods, it is concluded that the kaolin minerals from the Kasuga mine are composed of nacrite, dickite and kaolinite. It is of great interest that comparatively pure nacrite clay occurs in fissures in silicified rock at the latest stage of mineralization.

Acknowledgements

The writer wishes to record here his sincere thanks to Prof. Dr. T. Watanabe, University of Tokyo and Prof. Dr. T. Sudo, Tokyo University of Education, for their kind guidance and suggestions, and also for the reading of his manuscript. He wishes also to thank Mr. Y. Sekine, Geological Survey of Japan, for his kind criticism and also to Messrs. H. Mukaiyama and A. Sasaki for their encouragement.

He is also very much indebted to the officials of the Nippon Mining Co. Ltd. and of Kasuga Mine, especially to Messrs. S. Nishizawa, S. Ôbayashi, Y. Inokuchi and T. Kuchii.

He also wishes to express his gratitude for the grants from the Scientific Research Fund of the Department of Education during 1950~1953 which enabled him to carry on a part of his field and laboratory work.

References

1) Brindley, G.W.: X-ray Identification and Crystal Structures of Clay Minerals, London (1951).
2) Claringbull, G.F.: Min. Mag., **29**, 973 (1952).
3) Gruner, J.W.: Zeits. Krist., **85**, 345 (1939).
4) Grim, R.E. and R.A. Rowland: Am. Mineral., **27**, 746 & 801 (1942).
5) Grim, R.E.: Clay Mineralogy, New York (1953).
6) Iwai, S., H. Takeshi and J. Ossaka: Jour. Japan Assoc. Min. Pet. & Econ. Geol., **33**, 169 (1949). (in Japanese)
7) Kerr, P.F., J.L. Kulp and P.K. Hamilton: Amer. Petroleum Inst. Project 49, Clay Mineral Standard Pre. Rep. 3 (1949).

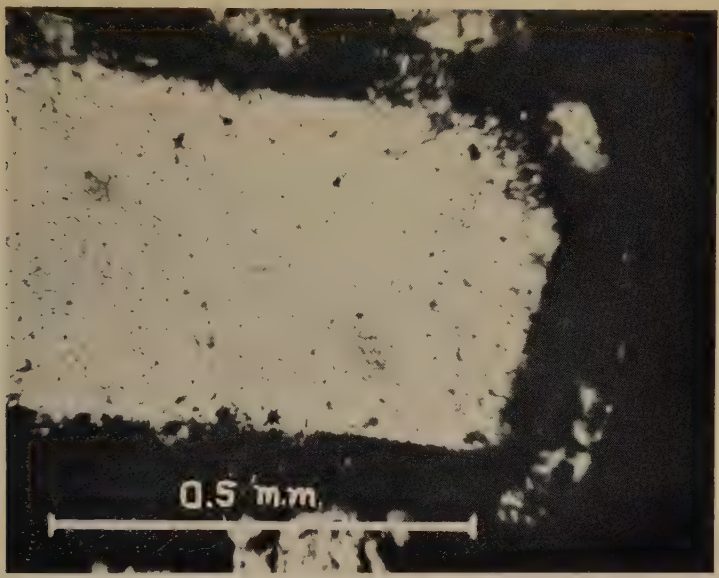

Fig. 3a. Dickite aggregates replacing the phenocrysts of original rocks.

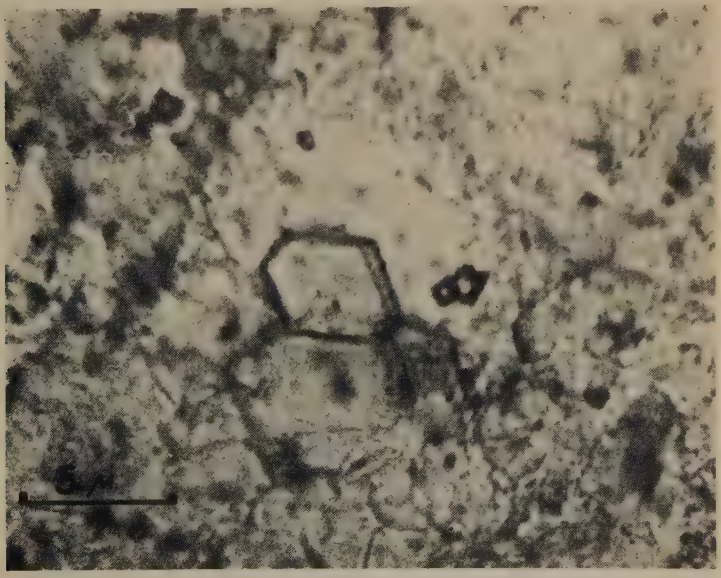

Fig. 3b. Well formed flaky crystals of dickite from the Kasuga mine.

8) Kerr, P.F.: Am. Petroleum Inst. Proj. 49, Pre. Rept. 7, 160 (1950).
9) Knorring, O. Von, G.W. Brindley and K. Hunter: Min. Mag., **29**, 963 (1952).
10) Norton, F.H.: Jour. Am. Ceramic Soc., **22**, 54 (1939).
11) Nagelschmidt, G.: Zeits. Krist., **87**, 120 (1934).
12) Ross, C.S. and P.K. Kerr: U.S. Geol. Surv. Prof. Paper 165 E, 151 (1931).
13) Sudo, T., K. Nagasawa, M. Amafuji, M. Kimura, S. Honda, T. Muto and M. Tanemura: Jour. Geol. Soc. Japan, **58**, 115 (1952).
14) Tokunaga, M.: Jour. Soc. Mining Geologists Japan, **4**, 205 (1954). (in Japanese)
15) Tokunaga, M.: Jour. Soc. Mining Geologists Japan, **5**, 1 (1955). (in Japanese)

Manuscript received April 10, 1956.

Mineralogical Journal, Vol. 2, No. 2, pp. 114–133, June, 1957

ON PROBABLE ELLIPTIC VIBRATION OF LIGHT IN HEIKOLITE*

Tokugoro Shoda

Mineralogical Institute, University of Tokyo

Abstract

It is concluded that the anomalous optical property of heikolite may be due to the elliptic vibration of light wave, resulting from the strong absorption of the mineral.

The formula for calculating the intensity of emerged light was introduced and the orientations of the major axes and the axial ratios of the ellipses, the reduction ratios of amplitudes of light wave, and the phase difference between the two elliptically polarized waves in the crystal, were determined with the heikolite section parallel to (010).

The intensity curves obtained from observations were in good accordance with those obtained from calculations.

Introduction

The (010) section of some alkali amphiboles does not extinguish between crossed nicols even with the monochromatic light. Concerning the anomalous optical properties of alkali amphiboles, many studies[1)10)11)14)] were made in the past fifty years.

For example, Eskola and Schalstein[1)] studied some alkali amphiboles and considered that they are not homogeneous but are perthitic. Similar anomalous optical properties were noticed also by a number of Japanese authors[2)3)4)5)7)8)9)17)].

Hori[3)], especially, made quantitative optical measurements on heikolite from Koganzan in Korea, and in order to explain the

* Read at the joint meeting of the Mineralogical Society of Japan, the Japanese Association of Mineralogists, Petrologists and Economic Geologists, and the Society of Mining Geologists of Japan, held in Sendai on October 6, 1956.

result, assumed that the mineral consists of two sets of parts, each set with definite but mutually different orientation. According to his assumption, when the light passes through the (010) section of heikolite, one of the linearly polarized waves in each part is entirely absorbed, and two linearly polarized waves with their vibration directions making some oblique angle come out. The angle between the two vibration directions was determined by him as 42°.

Recently, optical, chemical and X-ray studies were made by Sahama[11] on arfvedsonite from Kangerdluarsuq in Greenland. He concluded that the anomalous optical property of the mineral is due to the perthitic intergrowth of two amphiboles, with slightly differing unit cell dimentions.

The present writer[12,13] made an experimental study on heikolite from Kansenri in Korea. The light transmitted through the (010) section of the mineral was measured with a photometer for various wavelengths, and the intensity curves obtained were compared with that for aegirine, which is strongly pleochroic but shows normal extinction between crossed nicols. Further, the dependence of the absorption of heikolite on its orientation was determined. The results show that the orientation of the absorption axes differs much from that of the axes of indicatrix.

While the remarkable anomalous property of heikolite, as above, may be due to the perthitic structure, as considered by some previous authors, it is possible to be due to the elliptic polarization, as suggested by W. Voigt who showed theoretically that the absorptive biaxial mineral generally give rise to two elliptically polarized waves.*

The following work was undertaken in order to examine the ellipticity of vibrations in this mineral and to check its homogeneity.

Theoretical considerations

Let $A_0 \sin \tau$ be the vibration of the linearly polarized light pass-

* F. Pockels: Lehrbuch der Kristalloptik, p. 377.

ing through the polarizer whose vibration direction is represented by OP in Fig. 1. Upon entering the section, this vibration is resolved into two elliptic vibrations, with their major axes at right angle to each other and parallel or perpendicular to the definite crystallographical directions X''', Z''' in the section. The two ellipses are equal in axial ratio ϵ and have the same rotation sign (right in Fig. 1). When the two waves pass through the section, the intensities of the two elliptic vibrations decrease according to the normal absorption formula $e_1=e^{-m_1 d}$, $e_2=e^{-m_2 d}$ so that the axial ratios of both ellipses do not change throughout the whole path. At the emergence, phase of one elliptic vibration differs by Δ from that of the other. The resultant intensity of the emerged waves is given by

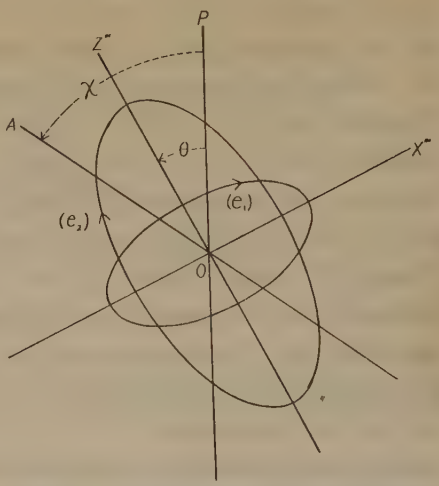

Fig. 1. Diagram showing the principal axes X''' and Z''' of the elliptic vibrations.
P: Vibration direction of polarizer.
A: Vibration direction of analyzer.

$$I=\frac{A_0^2 e_0^2}{(1-\epsilon^2)^2}\left\{A'\sin^2\theta+B'\cos^2\theta+C'\sin 2\theta\right\} \quad \cdots\cdots\cdots \quad (1)$$

where
$$A'=(1+\epsilon^2)(e_1^2+e_2^2\epsilon^2)-4e_1e_2\epsilon^2\cos\Delta,$$
$$B'=(1+\epsilon^2)(e_2^2+e_1^2\epsilon^2)-4e_1e_2\epsilon^2\cos\Delta,$$
$$C'=-2e_1e_2\epsilon(1-\epsilon^2)\sin\Delta$$

and e_0^2 is the reduction ratio of intensity through the optical parts. When the sign of ϵ is positive, equation (1) corresponds to that for the right handed elliptic vibration, and when it is negative, left handed.

The intensity, given by equation (1), takes its extreme value

when

$$\tan 2\theta = \frac{2\varepsilon}{1+\varepsilon^2} \cdot \frac{2e_1e_2 \sin \Delta}{e_1^2 - e_2^2} \quad \cdots\cdots\cdots\cdots (2)$$

and, if $\varepsilon > 0$, $\sin \Delta > 0$ and $e_2 > e_1$, the minimum position is situated between $\frac{\pi}{2} > \theta > \frac{\pi}{4}$.

If the emerged waves are brought back to the same vibration direction OA of the analyzer, which makes angle χ to OP, the intensity of light through the analyzer is given by the following equation, where e_a is the reduction ratio of amplitude by absorption or reflection through the analyzer and other optical parts.

$$I = \frac{A_0^2 e_a^2}{(1-\varepsilon^2)^2} \Big\{ A \sin^2(2\theta - \chi) + B \sin^2\theta \sin^2(\chi - \theta) + C \cos^2\theta \cos^2(\chi - \theta) + D \sin\theta \cos\theta \sin(\chi - \theta) \cos(\chi - \theta) + E \sin(2\theta - \chi) \Big\} \quad \cdots\cdots\cdots\cdots (3)$$

where
$A = \varepsilon^2(e_1^2 + e_2^2 - 2e_1e_2 \cos \Delta)$,
$B = e_1^2 + e_2^2\varepsilon^4 - 2e_1e_2\varepsilon^2 \cos \Delta$,
$C = e_2^2 + e_1^2\varepsilon^4 - 2e_1e_2\varepsilon^2 \cos \Delta$,
$D = 2\{(e_1^2 + e_2^2)\varepsilon^2 - e_1e_2 \cos \Delta(1+\varepsilon^4)\}$ and
$E = -2e_1e_2\varepsilon(1-\varepsilon^2) \sin \Delta \cos \chi$.

It will be seen from equation (3) that the curve of intensity variation with rotation of the stage for $\chi = \frac{\pi}{2}$ (crossed nicols) is symmetrical with respect to the positions with $\theta = 0, \frac{\pi}{4}, \frac{\pi}{2}, \cdots\cdots$, but the intensity does not become zero at these positions. The intensity will be minimum at $\theta = 0, \frac{\pi}{2}, \pi, \cdots\cdots$, and maximum at $\theta = \frac{\pi}{4}, \frac{3}{4}\pi, \cdots\cdots$. The value of the maximum or the minimum intensity is given by:

$$I_{max} = \frac{A_0^2 e_a^2}{(1-\varepsilon^2)^2} \cdot \frac{(\varepsilon^2+1)^2}{4} (e_1^2 + e_2^2 - 2e_1e_2 \cos \Delta)$$

or

$$I_{min} = \frac{A_0^2 e_a^2}{(1-\varepsilon^2)^2} \cdot \varepsilon^2(e_1^2 + e_2^2 - 2e_1e_2 \cos \Delta).$$

If an elliptic vibration, instead of linear, falls upon a crystal

section, it will pass through the section without changing its axial ratio and major axis direction under the following conditions. The major axis direction of the incident elliptic vibration is parallel to X''' or Z'''; its axial ratio is equal to that of the elliptic vibration in the section; its rotation sign is same as that of the elliptic vibration in the section. In these cases, the intensity of light through the section, without analyzer, is $A_0^2e_1^2$ or $A_0^2e_2^2$, the reduction of intensity through the optical parts being neglected.

The elliptic vibration with any desired axial ratio can be produced by passing a linearly polarized light through a quarter undulation plate. The axes of the ellipse are parallel to the vibration direction, X' and Z', of the $\frac{1}{4}\lambda$ plate. Denote by ψ the angle between the vibration direction of polarizer and that of X' of the plate, then the relation between ψ and ε will be given by

$$\tan\psi=\varepsilon. \qquad \cdots\cdots\cdots\cdots \quad (4)$$

If an elliptic vibration passing through the section falls on another $\frac{1}{4}\lambda$ plate whose vibration direction X' is parallel to the Z' of the first $\frac{1}{4}\lambda$ plate (the two $\frac{1}{4}\lambda$ plates are mutually in subtraction positions), the elliptic vibration will be converted to a linear vibration whose direction is parallel to that of the polarizer. Consequently, under such conditions, extinction of light takes place between crossed nicols.

If Z' of the second $\frac{1}{4}\lambda$ plate is superposed on Z' of the first (the two $\frac{1}{4}\lambda$ plates are mutually in addition positions), the elliptic vibration through the section will be converted to a linearly polarized one with its direction making angle 2ψ to the vibration direction of polarizer. In this case, the extinction occurs when the analyzer is rotated through 2ψ from its crossed position.

Fig. 2 shows the directions of Z' and X' in the first $\frac{1}{4}\lambda$ plate and those of Z''' and X''' in the section. The vibration directions of the second $\frac{1}{4}\lambda$ plate, put in subtraction position to the first, are represented by broken lines. The intensity of light that has passed through the polarizer, the first $\frac{1}{4}\lambda$ plate, the crystal

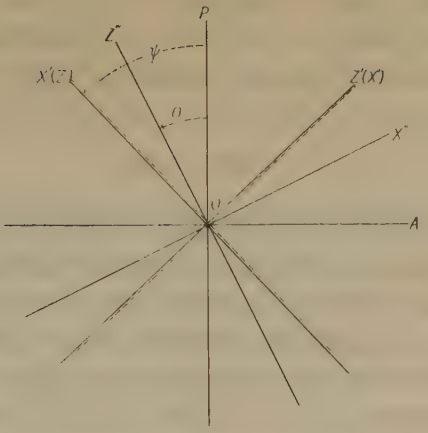

Fig. 2. Diagram showing the direction of X' and Z' of two $\frac{1}{4}\lambda$ plates superposed in subtraction position, between crossed nicols. Broken lines represent Z' and X' of the second $\frac{1}{4}\lambda$ plate.

section, the second $\frac{1}{4}\lambda$ plate and the analyzer successively, is given by the following equation.

$$I=\frac{A_0^2}{(1-\varepsilon^2)^2}\cdot\frac{e_1^2+e_2^2-2e_1e_2\cos\Delta}{4}\left[\sin^2 2(\psi-\theta)\left\{(1+\varepsilon^2)-2\varepsilon\sin 2\psi\right\}^2+\cos^2 2(\psi-\theta)\left\{2\varepsilon-(1+\varepsilon^2)\sin 2\psi\right\}^2\right]. \quad \cdots\cdots (5)$$

The intensity curve obtained from equation (5) shows that the same state occurs at every $\frac{\pi}{2}$ angle of rotation of the stage. The intensity becomes zero at $\theta=\psi$ and $\tan\psi=\varepsilon$, viz. complete extinction takes place when the axial ratio and the principal axes directions of incident ellipse just coincide with those of the section. The intensity becomes minimum at $\theta=\psi$ and maximum at $\theta=\psi+\frac{\pi}{4}$. When $\psi=\pm\frac{\pi}{4}$, the intensity is independent of θ, taking the value of $\frac{1}{4}(e_1^2+e_2^2-2e_1e_2\cos\Delta)(1-\varepsilon)^4$ for the right handed incident wave, and the value of $\frac{1}{4}(e_1^2+e_2^2-2e_1e_2\cos\Delta)(1+\varepsilon)^4$ for the left handed.

Therefore, if the elliptic vibration in the section is right handed ($1>\varepsilon>0$), the intensity for the left handed incident wave is much stronger than that for the right handed.

Experimental

A heikolite plate parallel to (010) face and a quartz plate parallel to the c-axis were cut. These were ground together to the thickness $d=0.030$ mm, and then ground again to $d=0.026$ mm., then to $d=0.016$ mm., and finally to $d=0.0096$ mm.. At each time, the thickness of the section was determined by means of the Soleil-Babinet compensator.

For examining whether the section of heikolite produces two elliptic vibrations, as supposed in the above explanation, it is necessary to prepare three rotation stages to put $\frac{1}{4}\lambda$ plates as well as section on. For this purpose, a couple of rotation stages was set above the stage of the polarizing microscope. The stage of the microscope and two attached stages rotate independently. In order to set the axes of all the three rotation stages exactly in the position of the axis of the microscope, the following procedure was taken. First, the centre of an attached stage was brought on the axis of the microscope by the usual method of centering. Next, one of the two $\frac{1}{4}\lambda$ plates was placed on the microscope, and the other on the attached stage. On rotating the stages independently, the two $\frac{1}{4}\lambda$ plates were brought to subtraction positions. If the planes of the $\frac{1}{4}\lambda$ plates, and accordingly the planes of the attached stages, are perpendicular to the axis of the microscope, complete extinction is to occur by bringing the two superposed $\frac{1}{4}\lambda$ plates to diagonal positions between crossed nicols; otherwise, no complete extinction. The positions of the stages were adjusted by observing complete extinction according to what has been stated above.

Throughout the whole experiments, a light with the wavelength of 587 mμ. from the monochromator was used. The deviation of

the values thus obtained from those for Na-light (D-line) is considered to be very small.

The intensity of light transmitted through the microscope was measured by a photometer which consists of a photomultiplier and a galvanometer[6].

Measurements with the (010) section between two $\frac{1}{4}\lambda$ plates

In order to examine whether the experimental results agree with what are derived from equation (5), one of the two $\frac{1}{4}\lambda$ plates was placed on the stage of microscope and the other on the upper attached stage. A (010) section of heikolite (d=0.0096 mm.) was placed on the lower attached stage, namely, between the two $\frac{1}{4}\lambda$ plates, and it was observed how the intensity of light that passed

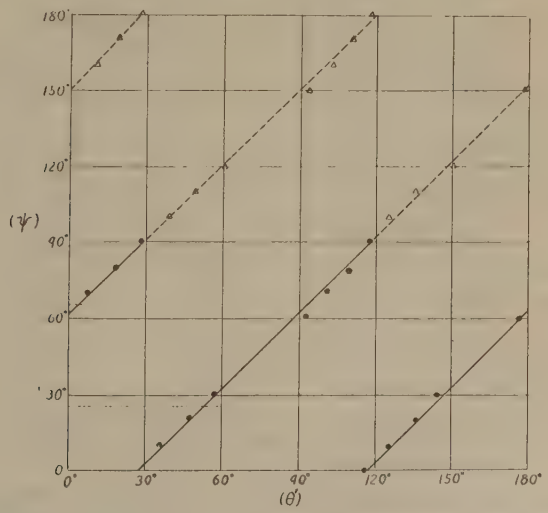

Fig. 3. Positions of the minimum intensity for various positions of two $\frac{1}{4}\lambda$ plates. (Crossed nicols)

● and full lines: Incident wave has right handed polarization.

△ and broken lines: Incident wave has left handed polarization.

ψ: Angle between the vibration direction of polarizer and X'.

θ': Angle between the cleavage trace and the vibration direction of polarizer.

through the above system varies with rotation of the stage between crossed nicols. The measurements were made at various positions (given by angle ψ) of the $\frac{1}{4}\lambda$ plates and the values of the minimum intensity and the corresponding positions were determined. These were plotted in a diagram as shown in Fig. 3.

The positions of the minimum intensity lie approximately on two straight lines making 45° to the abscissa, and the abscissa value of one line corresponding to a definite ordinate value differs by nearly 90° from that of the other line.

Fig. 4 shows the relation between the value of the minimum intensity and that of ψ. The curve on the left side of the figure represents the minimum intensity variation when the angle ψ varies

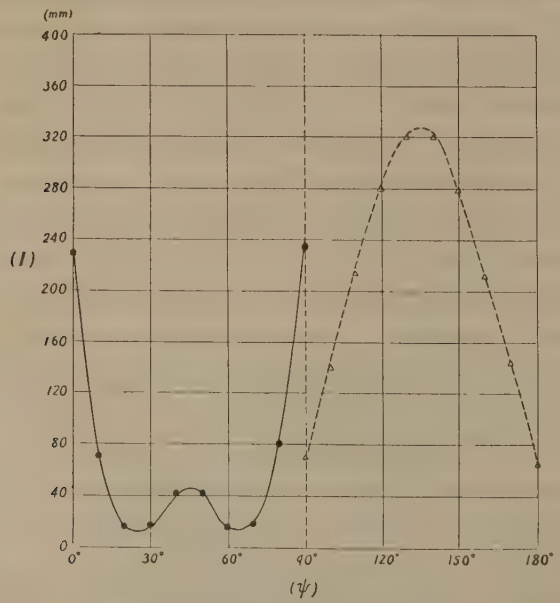

Fig. 4. The values of the minimum intensity for various positions of two $\frac{1}{4}\lambda$ plates. (Crossed nicols)

● and full lines: Incident wave has right handed polarization.

∧ and broken lines: Incident wave has left handed polarization.

I: Scale readings on the galvanometer.

ψ: Angle between the vibration direction of polarizer and X'.

from 0° to 90°, that is, when the incident polarized wave is right handed. The curve on the right side, on the other hand, corresponds to the case where the incident wave is left handed.

As is evident from the figure, the intensity is much stronger when the incident light has left handed circular polarization, than when it has right handed. This difference is more directly illustrated by the microphotographs shown in Fig. 16 (Plate II). For the sake of comparison, the photographs of the (010) section of aegirine are shown in Fig. 17 (Plate II).

The curve in Fig. 4 shows that the intensity becomes nearly zero at the position corresponding to $\psi=25°$ or $\psi=65°$, where the direction of the major axis of the incident elliptic vibration is parallel to X''' or Z''' in the section, and the axial ratio of the incident ellipse is equal to ε in the section. From equation (4), the value of ε for this section was calculated as:

$$\varepsilon=+0.466.$$

The abscissa values corresponding to the ordinate value of 25° or 65° give the orientation of X''' or Z''' in the section.

However, the orientation of X''' or Z''' can be more accurately determined from the intensity curve for crossed nicols, of which explanation will be given in the following chapter. Fig. 5

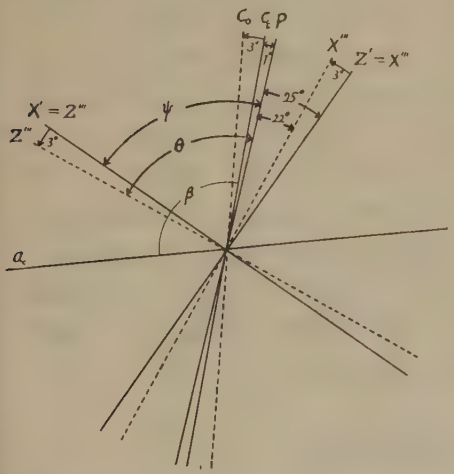

Fig. 5. The orientation of X''' and Z''' with respect to the cleavage trace in the section (010).

ψ: Angle between the vibration direction of polarizer and X'.

θ: Angle between the vibration direction of polarizer and Z'''.

C_c: Direction of the cleavage trace when the intensity becomes minimum for the case with crossed nicols.

C_o: Direction of the cleavage trace when the intensity becomes minimum for the case with polarizer only.

shows the orientation of X''' and Z''' with respect to the cleavage trace in the section.

The measurements were also made for the section between two $\frac{1}{4}\lambda$ plates, whose vibration directions were in addition positions. The $\frac{1}{4}\lambda$ plates were put in fixed positions ($\psi=25°$ or $\psi=65°$), and the section was turned to bring its X''' and Z''' respectively parallel to X' and Z' of the $\frac{1}{4}\lambda$ plates. The intensity of light was measured

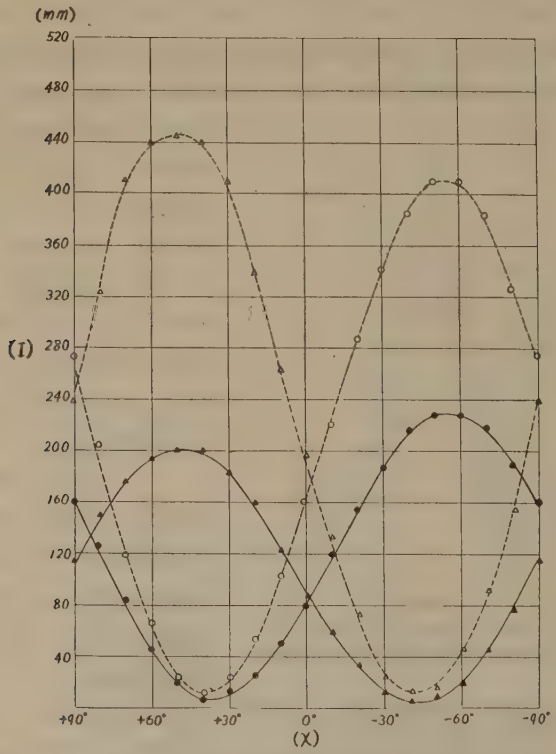

Fig. 6. Intensity curve with χ when the directions of X' or Z' of two $\frac{1}{4}\lambda$ plates which are in addition positions just parallel to X''' or Z''' in the section.

●: $\psi=65°$ and $\theta'=1°$. ○: $\psi=65°$ and $\theta'=91°$.

▲: $\psi=25°$ and $\theta'=51°$. △: $\psi=25°$ and $\theta'=141°$.

ψ: Angle between the vibration direction of polarizer and X'.

θ': Angle between the cleavage trace and the vibration direction of polarizer,

successively for various χ angle, and the results as shown in Fig. 6 was obtained. As is easily seen in the figure, the intensity is nearly zero at $\chi \fallingdotseq \pm 40°$.

Determination of e_1 and e_2

The $\frac{1}{4}\lambda$ plate on the upper attached stage was removed and the intensity of light without analyzer was measured. The values of e_1 or e_2 were determined as follows. The scale readings on the galvanometer without mineral section on the stage were found to be

$$A_0^2 e_a^2 (1-R)^2 = 210 \text{ mm.},$$

where R is the reflection power of glass to air.

For $\psi = 65°$ and $\theta' = 1°$, $A_0^2 e_a^2 (1-R)^2 (1-R')^2 e_1^2 = 20$ mm.;

for $\psi = 65°$ and $\theta' = 91°$, $A_0^2 e_a^2 (1-R)^2 (1-R')^2 e_2^2 = 60$ mm.;

where R' is the reflection power of glass to mineral.

For $\psi = 25°$ and $\theta' = 51°$, $A_0^2 e_a^2 (1-R)^2 (1-R')^2 e_1^2 = 22$ mm.;

for $\psi = 25°$ and $\theta' = 141°$, $A_0^2 e_a^2 (1-R)^2 (1-R')^2 e_2^2 = 57$ mm..

Assuming that the scale readings on the apparatus are proportional to the light intensity to be measured, and that the refractive indices of the glass and the mineral are 1.5 and 1.68 respectively, the values of e_1 and e_2 were calculated as follows:

$$e_1 = 0.319, \quad e_2 = 0.531.$$

Determination of Δ

As there is no direct means of determining the value of Δ, it was determined from the minimum position of the intensity curve obtained from the measurements with the polarizer only, by use of equation (2). For the section used in this experiment, we obtained an intensity curve similar to that obtained for the section reported in the previous paper[12].

From the intensity curve for the polarizer only shown in Fig. 7, the position of the minimum intensity was found to be at $\theta' = 4°$ in the rotation angle of the cleavage trace. Therefore, the position of

the minimum intensity for the rotation angle of Z''' direction is given as $\theta=68°$ (Fig. 5). Substituting ϵ, θ, e_1 and e_2 in equation (1) for the values obtained above, the value of Δ was calculated as:

$$\Delta=40° \ 10'.$$

Comparison of observed and calculated intensity curves

The curve obtained from the measurements with the polarizer only shows the behaviour symmetrical with respect to the positions of the maximum and the minimum as shown in Fig. 7. However,

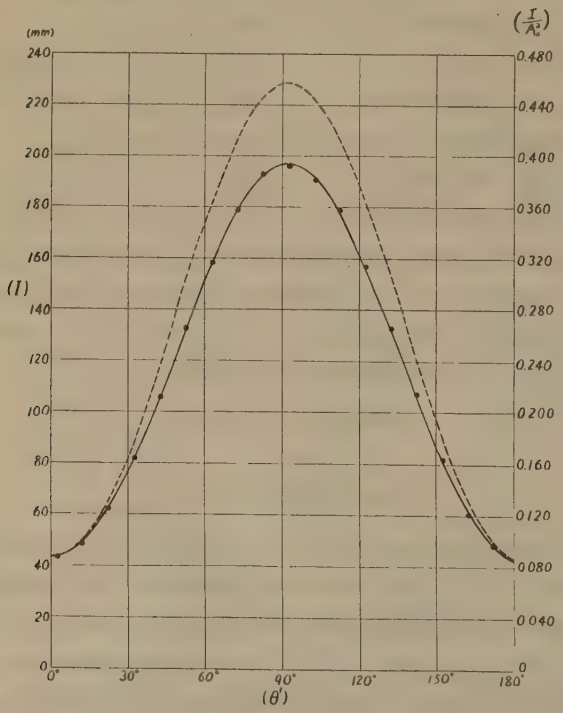

Fig. 7. Intensity variations for the (010) section with the polarizer only.
Full line: Observed; I: Scale readings on the galvanometer.
Broken line: Calculated; $\frac{I}{A_0^2}$: Calculated intensity.

the curve expected theoretically from equation (3) must be asymmetric owing to the fact that the last term of the equation contains 2θ angle. But the calculated curve using the above values of ε, e_1, e_2 and Δ is symmetrical as shown by broken line in Fig. 7, and is similar with that obtained from the observation. It is inferred that there is no appreciable effect of the last term when the value of e_2 much differs from that of e_1.

The intensity curve, obtained in this experiment, for the section between crossed nicols, is similar to that reported previously[12]. It is symmetrical with respect to the positions of the maximum and the minimum, and the repetition occurs at every $\frac{\pi}{2}$ angle of θ'. In Fig. 8, the observed curve is shown by full line, and the calculated curve,

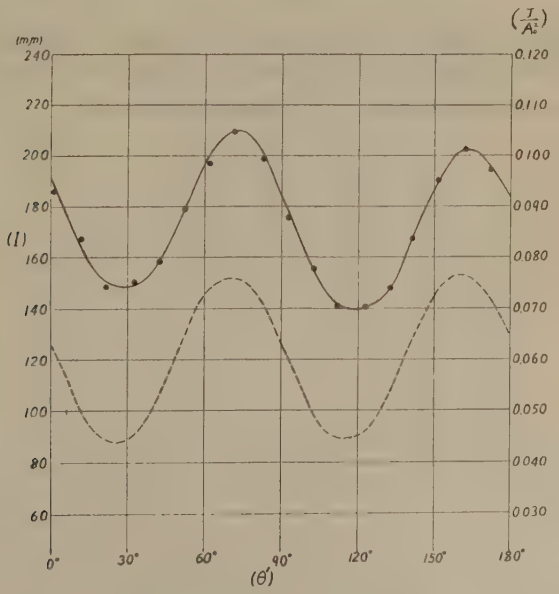

Fig. 8. Intensity variation for the (010) section with crossed nicols.

Full line: Observed; I: Scale readings on the galvanometer.

Broken line: Calculated; $\frac{I}{A_0^2}$: Calculated intensity.

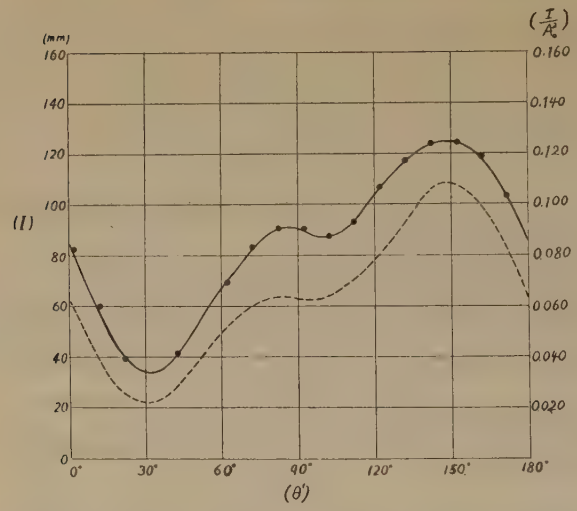

Fig. 9. Intensity variation for the (010) section. ($\chi = 80°$)
Full line: Observed; I: Scale readings on the galvanometer.
Broken line: Calculated; $\frac{I}{A_0^2}$: Calculated intensity.

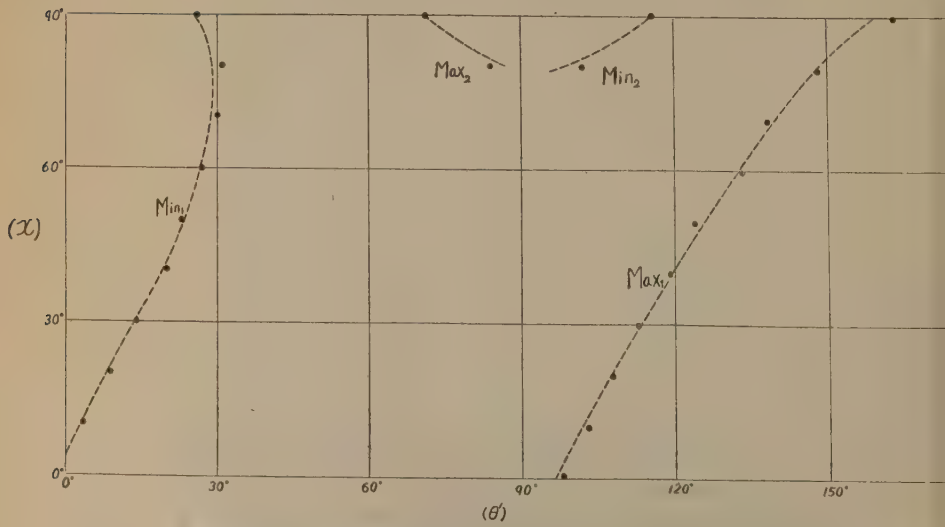

Fig. 10. Positions of maximum and minimum intensity for the (010) section.
Dots: Observed.
Broken lines: Calculated.

by broken line.

Fig. 9 shows the intensity curve for $\chi=80°$. Fig. 10 shows the positions of Min_1, Max_2, Min_2 and Max_1 for various χ angles. The variations with χ of the values of Min_1, Max_2, Min_2 and Max_1 are shown in Fig. 11. As is evident in these figures, the observed values are in good accordance with the calculated values.

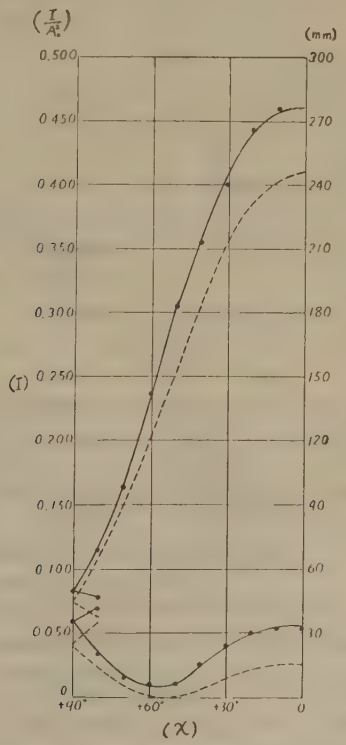

Fig. 11. Variation of the values of maximum and minimum intensity for the (010) section.
Full lines: Observed.
Broken lines: Calculated.

Variations in the optical behaviour with the thickness

The intensity measurements were also made with three sections

of different thickness, d=0.016 mm., 0.026 mm. and 0.030 mm., and the positions of the maximum and the minimum intensity determined were compared with those obtained by calculation from the above data at hand. Fig. 12 shows the positions of the minimum intensity in the case with the polarizer only and Fig. 13 shows the

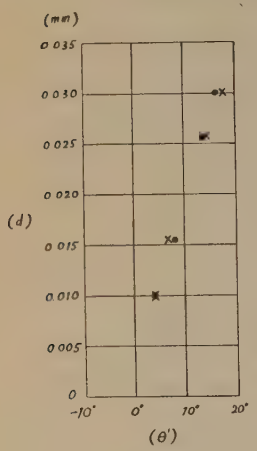

Fig. 12. Variation of the positions of minimum intensity with thickness. (Polarizer only)

- ●: Observed.
- ×: Calculated.
- d: Thickness of the section.
- θ': Rotation angle of the section.

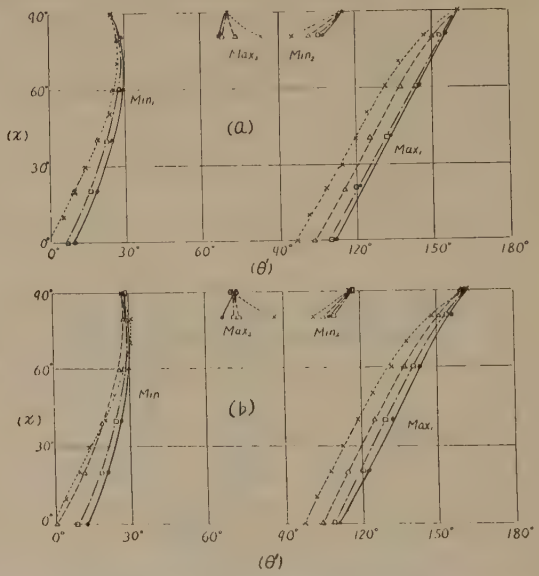

Fig. 13. Variation of the positions of maximum and minimum intensity with thickness.

(a) Calculated. (b) Observed.

- × and dotted lines: d=0.0096 mm.
- △ and broken lines: d=0.016 mm.
- □ and chains : d=0.026 mm.
- ● and full lines : d=0.030 mm.

results in the case where the nicols are oblique to each other. In Fig. 13, it can be seen that the effects of variations in thickness on the curves in (a) and (b) are similar to each other.

In Fig. 14, comparison is made of the curves of Min_1 *versus* χ as observed and as calculated for various thickness. For the section with d=0.0096 mm., when χ changes from 90° to 0°, the minimum

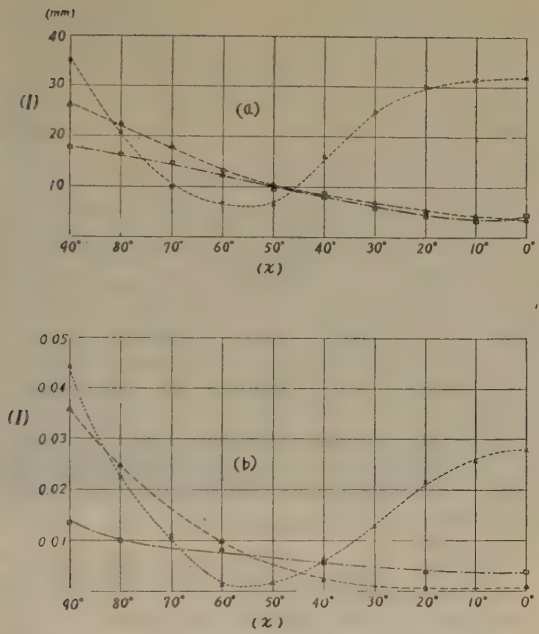

Fig. 14. Variation of the intensity of Min_1 *versus* χ curve with thickness.

(a) Observed. (b) Calculated

× and dotted lines: $d=0.0096$ mm.

△ and broken lines: $d=0.016$ mm.

□ and chains : $d=0.026$ mm.

intensity decreases to $\chi \fallingdotseq 55°$, but again increases with further decrease of χ. However, the value of χ corresponding to the minimum intensity decreases as the thickness of the section increases. For the section with $d=0.016$ mm., the minimum intensity is nearly zero in the range of $\chi=0°\sim20°$.

X-ray investigations

In order to examine whether the sample of heikolite in question has the perthitic structure or not, zero-level precession photographs were taken by M. Korekawa of the sample which is abnormal in extinction, using molybdenum radiation without filter. The preces-

sion angle was 30°; magnification factor was 60 mm.. The photographs showing the projections of three reciprocal lattice planes (a* b*), (b* c*) or (a* c*) were taken. The projection of (a* b*), for example, is illustrated in Fig. 15 (a) (Plate I) and the corresponding reciprocal lattice net for $K\alpha$ is shown in Fig. 15 (b) (Plate I), in which the strong, medium and weak reflections are represented by the large, medium and small size of solid circles respectively.

These photographs show that there is only one sort of reciprocal lattice. There is no indication for the coexistance of differently orientated crystals or of more than one phase of different unit cell dimentions.

The lattice constants of this mineral calculated from the photographs, are shown in Table 1, together with the data of other amphiboles described previously.

Table 1. Lattice constants of amphiboles.

	tremolite[15]	crocidolite[16]	actinolite[18]	heikolite
a	9.78Å	9.89Å	9.89Å	10.0Å
b	17.80	17.95	18.14	18.0
c	5.26	5.31	5.31	5.33
β	106°02′	107°30′	105°48′	106°50′

Summary and conclusion

In order to examine the ellipticity of vibration in heikolite crystal, its (010) section was observed between two $\frac{1}{4}\lambda$ plates using the polarizing microscope with three rotation stages. The monochromatic light of the wavelength 587 mμ. was used in the experiment. The intensity of light transmitted was measured by a photomultiplier-galvanometer-set. From the results of the measurements, the orientations of the major axes and the axial ratios of ellipses, reduction ratios of amplitudes and phase difference in the light waves were determined. The intensity curves and the positions of the maximum and the minimum intensity for various χ angle obtained from the

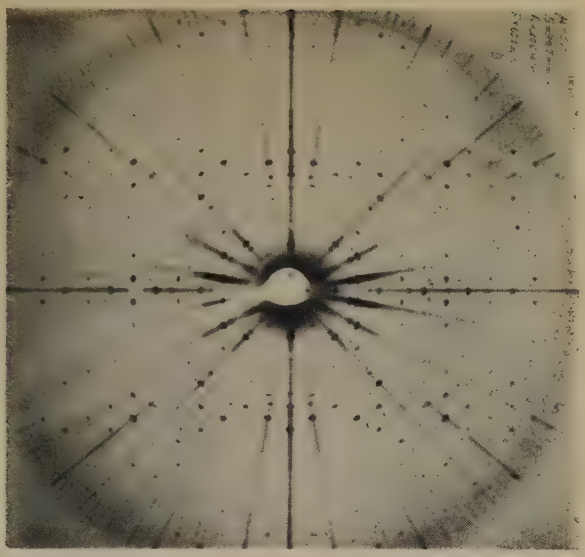

Fig. 15 (a). Precession photograph of heikolite, precessing about c-axis, using molybdenum radiation without filter. $\mu=30°$, $F=60$ mm., $s=34.7$ mm., $r_s=20$ mm.

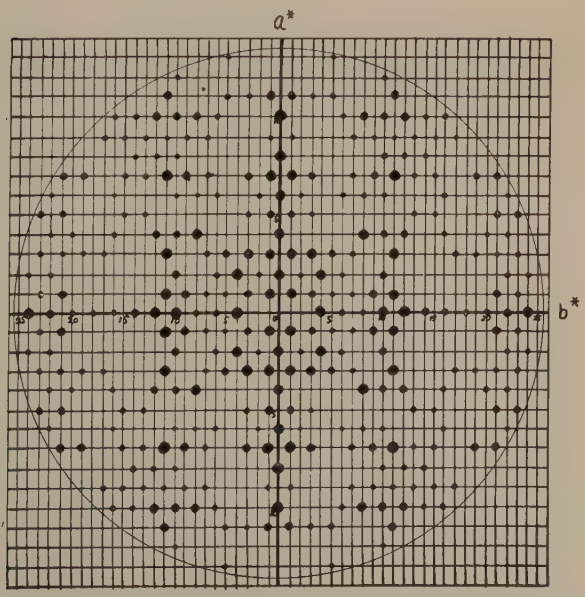

Fig. 15 (b). Projection of the reciprocal lattice net plane (a* b*) for $K\alpha$ to fit (a). The intensity of the spots is represented by the size of solid circles.

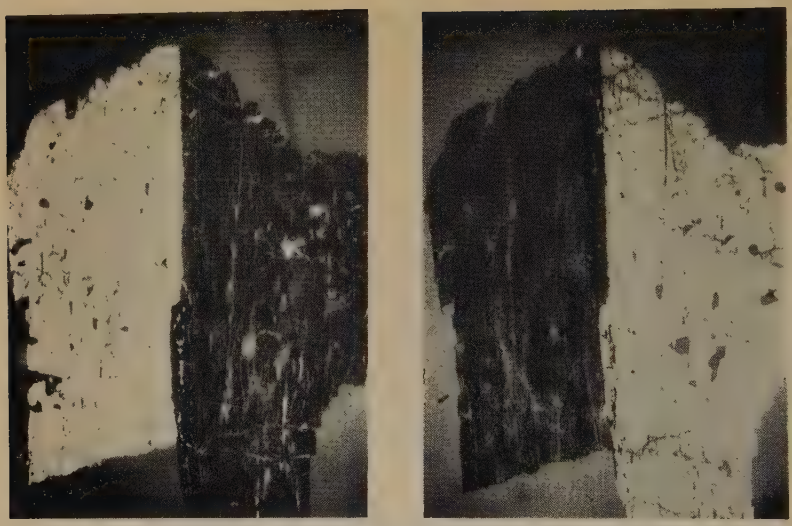

Fig. 16. Microphotographs of the (010) section of heikolite, twinned on c-axis, showing the dependence of the intensity on the rotation sign of incident wave. (Na D-line was used)
Left : Incident light has right handed circular polarization.
Right: Incident light has left handed circular polarization.

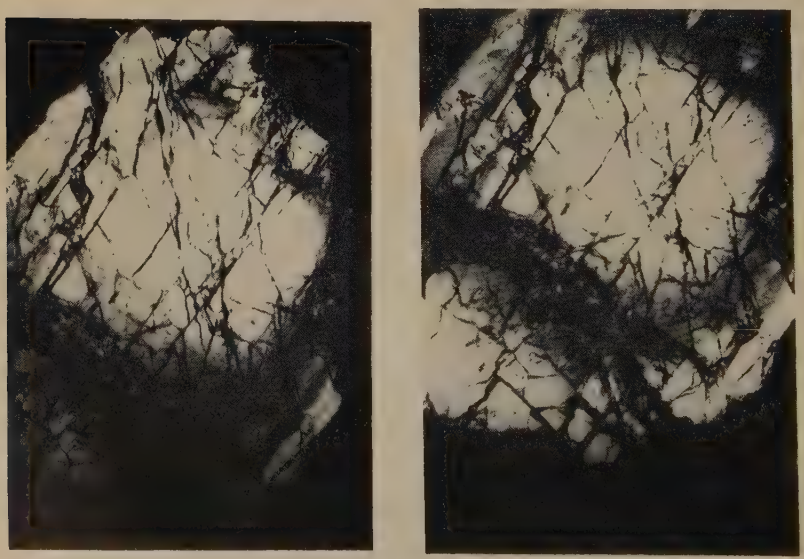

Fig. 17. Microphotographs of the (010) section of aegirine, showing the independence of the intensity on the rotation sign of incident wave. (Na D-line)
Left : Incident light has right handed circular polarization.
Right: Incident light has left handed circular polarization.

observations without the $\frac{1}{4}\lambda$ plate were found to be in good accordance with those obtained from calculations.

X-ray precession photographs did not show the doubling of spots, hence the mineral is considered to be of single phase. It is concluded that the anomalous optical properties of heikolite may be due to the elliptic vibrations of light, resulting from the strong absorption in the mineral.

Acknowledgements

The writer give his sincere thanks to Professor T. Ito, Mineralogical Institute, and Professor N. Katayama, College of General Education for their encouragements during this work. He is also indebted to Dr. R. Sadanaga and Dr. A. Miyashiro for criticisms and discussions. Special thanks are due to Mr. M. Korekawa of this Institute for taking the X-ray photographs. For preparation of sections, the writer owe to Mr. T. Watanabe of the Earthquake Resarch Institute.

REFERENCES

1) Eskola, P. and T.S. Schahlstein: Bull. Comm. Geol. Finland, **92**, 89 (1930).
2) Harada, Z.: Jour. Geol. Soc. Jap., **46**, 291 (1939). (in Japanese)
3) Hori, S.: Jour. Geol. Soc. Jap., **49**, 445 (1942). (in Japanese)
4) Inoue, T.: Jour. Geol. Soc. Jap., **56**, 71 (1950).
5) Iwao, S.: Jap. Jour. Geol. Geogr., **16**, 155 (1939).
6) Katayama, N. and Y. Sato: Jour. Miner. Soc. Jap., **1**, 73 (1953). (in Japanese)
7) Kinosaki, Y.: Chosen-Kobutushi, 198 (in Japanese).
8) Kinosaki, Y.: Jour. Mining Assoc. Korea, **18**, 187 (1935). (in Japanese)
9) Miyashiro, A.: Jour. Fac. Sc., Univ. Tokyo, Sec. 2, **10**, 50 (1956).
10) Morozewicz, J.: Tschermaks Miner. Petr. Mitt., **38**, 210 (1925).
11) Sahama, T.G.: Amer. Miner., **41**, 509 (1956).
12) Shoda, T.: Miner. Jour., **1**, 69 (1954).
13) Shoda, T.: Miner. Jour., **2**, 39 (1956).
14) Vendl, A.: Zeit. Krist., **60**, 135 (1924).
15) Warren, B.E.: Zeit. Krist., **72**, 42 (1930).
16) Whittakar, E.J.W.: Acta Cryst., **2**, 312 (1949).
17) Yagi, K.: Bull. Geol. Soc. America, **64**, 769 (1953).
18) Zussman, J.: Acta Cryst., **8**, 301 (1955).

Manuscript received March 15, 1957.

MINERALOGICAL JOURNAL, VOL. 2, NO. 2 pp. 134-137, JUNE, 1957

SHORT COMMUNICATIONS

NATURAL OCCURRENCES OF ZEUNERITE

KITINOSUKE HENMI

Institute of Earth Science, Faculty of Science,
University of Okayama

The torbernite and metatorbernite minerals have the formula $A(UO_2)_2(XO_4)_2 \cdot nH_2O$, where A is Cu, Ca, Ba or Mg, X is P or (sometimes and) As, and the values of n are about 10 in the torbernites while 8 or less in the metatorbernites.

As to the zeunerite minerals [$Cu(UO_2)_2(AsO_4)_2 \cdot nH_2O$], most of museum specimens belong to metazeunerite isostructural with metatorbernite, so the name zeunerite was used by J.W. Frondel[1] and also by the present writer[2] as a substitute for metazeunerite, while in the Dana's System of Mineralogy (1951) it was held in reserve status for natural occurrence of the mineral isostructural with torbernite.

In the autumn of 1956, a green uranium mineral offered by N. Katayama who had found it in the Suisho-yama* pegmatite, Fukushima Prefecture, was proved to be zeunerite (not metazeunerite) by X-ray and optical means. Then the fresh specimens from a humid gallary of the Miyoshi mine**, Okayama Prefecture, of which naturally dehydrated crystals had been known as metazeunerite[2], were tested and made clear that the specimens also reserved the zeunerite structure.

In this preliminary report, only some data directly related to the identification of this mineral are described; the detailed paper will

* 水晶山　　** 三吉鉱山

be written after further experiments.

Localities (1) Suisho-yama lies in the Town of Kawamata, Fukushima Prefecture, one of the most famous pegmatite regions in Japan. There are found considerable amounts of fergusonite, yttrialite, and other uranium minerals. Zeunerite occurs filling cracks of the lepidomelane zone remarkably rich in these uranium minerals.

(2) The Miyoshi mine is one of the tungsten mines in the northern part of Kurashiki City, Okayama Prefecture. Wolframite, arsenopyrite, chalcopyrite, molybdenite, cassiterite and other ore minerals are found in quartz veins in granite which is frequently greisenized. Tiny crystals of zeunerite are observed in the fissures of the deposits accompanied with other secondary minerals of copper and/or arsenic.

Composition The partially dehydrated crystals (metazeunerite) from Miyoshi were analyzed by K. Nagashima with following result[2]; CuO 8.9%, UO_3 56%, As_2O_5 22%, H_2O (remn.) 13%; total 100%.

The chemical compositions of zeunerite crystals from the two localities were determined only spectroscopically; their spectroscopically detective components were revealed to be quite similar to those listed above.

Forms Zeunerite from the two localities occurs as tiny square tablets. The observed forms on the crystals from Miyoshi are $c\{001\}$, $m\{110\}$, $e\{011\}$, $o\{013\}$ and $l\{112\}$, where the indices are determined on the basis of the axial ratio $c=2.89$ obtained by X-ray means. The crystal forms of Suisho-yama zeunerite are composed of *c* and *e*.

Table 1. Optical data on zeunerite.

	Indices of refraction		Pleochroism	Optical character
Locality	Suisho-yama	Miyoshi	Suisho-yama & Miyoshi	Suisho-yama & Miyoshi
ω	1.611	1.612	yellowish green	Uniaxial negative
ε	1.59	1.589	nearly colourless	

Optics The indices of refraction measured by the immersion method are shown in Table 1.

J.W. Frondel[1] determined the indices of refraction of the synthetic zeunerites as follows.

Synthetic zeunerite	with 16 H_2O	with 10 H_2O	with 8 H_2O	with 5 H_2O
ω	1.602	1.610	1.645~1.648	1.654

Table 2. X-ray powder patterns of zeunerite and torbernite (Cu/Ni).

Zeunerite						Torbernite	
(1) Suisho-yama		(2) Miyoshi		(3) Synthetic		(4) Kurayoshi	
d	*I*	*d*	*I*	*d*	*I*	*d*	*I*
10.1Å	10	10.3 Å	10	10.65Å	10	10.2Å	10
6.7	3	6.68	4	6.86	5	6.7	3
						5.23	1
5.08	6	5.05	6	5.04	8	5.01	7
4.51	1	4.53	1	4.55	3	4.50	3
		4.34	v			4.28	½
		3.98	v			3.91	½b
3.57	10	3.57	10	3.59	9	3.56	10
3.36	4	3.36	6	3.39	7	3.33	5
3.15	1	3.15	1	3.18	2	3.09	1
		3.05	½	3.07	1		
2.92	4b	2.93	2	2.93	4	2.89	2b
		2.88	1	2.86	4		
2.72	2	2.74	1	2.73	3	2.72	2
2.52	2	2.53	3	2.54	4	2.50	2
2.47	2	2.46	3	2.47	4	2.41	2
				2.42	1		
		2.37	½	2.38	1	2.32	½
2.29	1	2.30	½	2.31	2		
2.25	1	2.25	3	2.27	3	2.23	3
2.19	4	2.19	3	2.19	4		
2.07	5	2.07	5	2.08	5		
		1.977	v	1.985	1		
1.915	5	1.919	4	1.926	6		
1.860	1	1.862	½	1.873	2		
1.789	4	1.789	4	1.797	5		

Intensities estimated visually. It seems, there are some differences between the estimation methods in (3) and in the others.

(1) Fukushima Prefecture, Japan. Collected by N. Katayama.
(2) Okayama Prefecture, Japan.
(3) $Cu(UO_2)_2(AsO_4)_2{\cdot}16H_2O$. After J.W. Frondel[1].
(4) Tottori Prefecture, Japan.

The values of ω of the specimens from the two Japanese localities are very close to that of synthetic zeunerite with $10H_2O$.

X-ray data In Table 2, the X-ray powder patterns of natural zeunerite are compared with those of synthetic zeunerite (after J.W. Frondel) and of torbernite; the results show that the crystal structure of natural zeunerite is nearly the same as of synthetic hydrated zeunerite and similar to that of torbernite. The lattice constants of zeunerite from Suisho-yama were calculated as

$$a_0=7.19\text{Å}., \qquad c_0=20.7\text{Å}., \qquad c_0/a_0=2.89.$$

A little interrogation remains in relation to the water contents, namely, the X-ray result coincides with that of synthetic zeunerite with $16H_2O$ (after J.W. Frondel), while from the optical data the mineral is seemed to be with $10H_2O$.

Alteration The crystal of zeunerite is dehydrated to metazeunerite slowly in the arid atmosphere and rapidly by heating.

Acknowledgement The author wishes to thank Professor Nobuo Katayama of the University of Tokyo, who kindly gave the specimens from Suisho-yama and read the manuscript. Thanks are also due to Professor Keiichi Omori of the Tohoku University for affording the opportunity for the writer to visit Suisho-yama.

References

1) Frondel, J.W.: Amer. Miner., 36, 249 (1951).
2) Henmi, K.: Journ. Miner. Soc. Japan, 2, 182 (1955). (in Japanese)

Manuscript received April 6, 1957.

ABSTRACT OF THE KOBUTSUGAKU ZASSHI,

JOURNAL OF THE MINERALOGICAL SOCIETY
OF JAPAN, VOL. 3, NO. 2,
February, 1957

Hydrothermal Reaction of Zeolites (pp. 107—123)

Ryôiti Kiriyama, Mitsue Koizumi,
Katsuhisa Yamada and Rikusaburo Kitagaki

The powder obtained by heating natrolite at 700°C. in atmosphere was used as the material for hydrothermal experiment. It was confirmed to be amorphous by the X-ray powder method.

The reactions between it and distillated water were studied in the temperature range between 150° and 300°C. and over various time durations from 6 to 144 hours. And the experiments were also carried out with various amounts of water enclosed in reaction vessels, the full capacity of the vessels being 18 cc.. Each reaction product was identified on the basis of the results obtained by the X-ray powder method, by thermal analyses and by the measurements of the loss of weight due to the dehydration of the zeolitic water.

The results of experiments at 150° and 200°C. revealed that although the natrolite lattice is reconstructed to some extent after 72 hours (150°C.) and 48 hours (200°C.), on further treatment at these temperatures, however, the lattice breaks down at 96 hours and 72 hours for 150°C. and 200°C. respectively, and finally after 120 hours at 150°C. and 96 hours at 200°C., rather imperfect lattices of natrolite and analcite are formed. On the contrary, above 225°C. the lattice of natrolite is scarcely reconstructed and only that of analcite is easily formed regardless of the reaction time.

The higher the water content in the reaction vessel, and the larger the amount of Na^+ ion dissolved into the aqueous medium from the original material, the less perfect is the lattice of the reactant. In alkaline mediu

the lattice of analcite is stable together with that of natrolite, but in acidic medium, there appears only natrolite lattice as the reaction product.

Glauconite from the Oga Peninsula, Akita Prefecture

(pp. 124—129)

Sakurô Honda

A number of glauconite granules was collected from the boring core at the east of Ichinomé-gata in the Oga Peninsula, Akita Prefecture. Sp. gr.: 2.52. Mean refractive index: 1.605. Chemical composition: SiO_2 49.30, Al_2O_3 5.13, Fe_2O_3 18.78, FeO 2.31, CaO 0.59, MgO 3.54, (K_2O+Na_2O) 5.78, $H_2O(-)$ 8.51, Ig. loss 6.14, total 100.18%. There are three endothermic peaks at 150°, 510° and 940°C., with a slight exotherm at 450°C. which may be due to iron sulphide sticking on the surface of the granules. The X-ray powder lines as well as the form of individual crystals under the electron-microscope, are in good accord with the previous data for glauconite.

Some Properties of the Clay from Arima (pp. 130—136)

Satoru Kakitani

Tertiary clay deposits containing plant fossils are widely distributed in Yamaguchi Village near the Arima spa, Hyogo Prefecture, overlying liparite and granite.

From the results of X-ray diffraction experiments, differential thermal analyses, and of electron-microscope observation, it is made clear that the clay deposits are composed mostly of montmorillonite with some impurities of albite and quartz. By using quinhydron electrode, the hydrogen ion concentration of the water dropped on the clay was measured to be 5.2 in pH in equilibrium after 1.5 hours.

Various sorts of cation-clay were made of the Arima clay by adsorbing Na, K, Mg or Ca respectively, and the viscosities of plastic slimes of them were measured. The order of viscosity is as follows: Na-clay>Mg-clay>Ca-clay> white natural clay>pink natural clay>K-clay. The basal spacings of those cation-clays differ from each other considerably, that is, of K-clay 12.69, of Na-clay 13.42, of Mg-clay 15.80 and of Ca-clay 15.88Å.

On an Experimental Condition Favourable for the Formation of Aragonite (pp. 137—145)

Zyunpei Harada and Masaru Goto

For the purpose of accounting for the genesis of aragonite, crystalline $CaCO_3$ was synthesized by the use of diffusion method in aqueous solutions of methanol, ethanol, glycol or glycerine of various consentrations, so that Ca^{2+} and CO_3^{2-} reacted slowly in them. Following results were obtained.

The rate of formation of aragonite varied with reference to the value of the dielectric constant of the solution from which they crystallized out. The lower the value of dielectric constant of the solution, the more favourable is the formation of aragonite. In the concentrated ethanol solution whose dielectric constant was as low as 55, nearly all crystals were formed as aragonite even at room temperature. When the dielectric constant of solution was about 60, almost equal amount of aragonite and calcite were formed. The influence of reaction velocity on the formation of aragonite is probably not so effective as it has been usually assumed.

Structural Changes of Schiller-Feldspar due to the Heat Treatment (II) (pp. 146—157)

Takeshi Tomisaka, Goro Shibuya and Hiroyuki Nakamura

Four specimens of schiller-feldspar, two of oligoclase and two of labradorite, were investigated to clarify the cause of their schillerization, which was inferred to be due to the reflection from minute hematite inclusions regulary distributed in, and genetically related to, their host crystal. The obtained results seem to support the inference in the following two point: (1) Schillering planes are (001), (010), (100), $(\bar{2}01)$ or the twinning plane of Pericline type, and parallel to them minute hematite crystals are distributed in all cases. (2) All of the four specimens belong to low-temperature plagioclase, and it was confirmed by optical and X-ray examination that they are inverted to high-temperature type by heating. This inversion is accompanied by the loss of the hematite inclusion as well as the fading of the schillerization.

Short Communications

Clay Minerals of Weathering and Sedimentary Origins from the Higashiyama District, Nagoya City (pp. 158—164)

Yoshiro Tsuzuki

Clay minerals and iron oxide minerals which are contained in the weathered gravel-beds and the silts in the Higashiyama district have been investigated. The species of iron oxide minerals and their amounts vary with the weathering conditions, while the essential clay minerals are in all cases halloysite which contains the hydrated form to some extent. The temperature of exothermic peak of D.T.A. curve of the clay minerals are higher for those in weathered gravels, lower for those in soils near the present surface of the earth, and intermediate for those in silts. This relation seems to be due to the degree of crystallinity as shown by their X-ray pattern and electron-micrographs.

Celestine from the Udô Mine, Shimané Prefecture (pp. 165—166)

Michitoshi Mukae

Celestine found in the epithermal gypsum deposit of the Udô mine, Shimané Prefecture, is fibrous, translucent and of pale blue colour. Hardness: 3.5. Sp. gr.: 3.961 at 4°C.. Spectroscopically pure $SrSO_4$. X-ray powder lines are in good accord with those of the celestine from England.

Reviews

X-RAC and S-FAC, Electronic Analogue Computers for X-ray Crystal Analysis ..... Yoshio Takéuchi ... 167—181

Proceedings ..... 185—186

Mineralogical Society of Japan

OFFICERS FOR 1957–1958

President: Teiichi Ito, University of Tokyo, Tokyo.

Vice-President: Bumpei Yoshiki, Asahi Glass Co. Ltd., Tokyo.

Secretary: Toshio Sudo, Tokyo University of Education, Tokyo. Keiichi Omori, Tohoku University, Sendai.

Treasurer: Tokugoro Shoda, University of Tokyo, Tokyo.

Editor: Nobuo Katayama, University of Tokyo, Tokyo.

Councillors: Zyunpei Harada; Hokkaido University, Sapporo. Keiichi Omori, Tsunehiko Takeuchi; Tohoku University, Sendai. Teiichi Ito, Shuichi Iwao, Nobuo Katayama, Eiichi Minami, Ryoichi Sadanaga, Tokugoro Shoda, Seitaro Tsuboi, Takeo Watanabe; University of Tokyo, Tokyo. Toshio Sudo, Tokyo University of Education, Tokyo. Teiroku Sueno, Onoda Cement Co. Ltd., Tokyo. Ichiro Sunagawa, Geological Survey of Japan, Tokyo. Kin-ichi Sakurai, Tokyo. Ryoiti Kiriyama, University of Osaka, Osaka. Kitinosuke Henmi, Okayama University. Okayama. Yoshio Kinosaki, Hiroshima University, Hiroshima. Kameki Kinoshita, Toyofumi Yoshimura; Kyushu University, Fukuoka.

PUBLICATIONS

Kôbutsugaku Zasshi, Journal of the Mineralogical Society of Japan

A journal containing articles and reviews on mineralogy and allied sciences contributed by members of the Mineralogical Society of Japan. Published every four months, in Japanese. Sent to all members of the Society. Membership dues $2.00 annually.

Mineralogical Journal

A journal containing articles on mineralogy and allied sciences, published semi-annually in English principally. Contributions are invited from everyone. The Journal completed its first volume of six numbers in 1956. Back numbers may be obtained at $1.00 per single copy for the time being. The price of subsrciption to the second volume is $5.00 per volume.

Printed by "HERALD" Printing Co., Ltd.